Master's Thesis of Agriculture

Polyethylenimine-conjugated Arabinogalactan for Hepatocellular Carcinoma Targeted Gene Delivery Systems

폴리에틸렌이민으로 개질한 간암 표적화 아라비노갈락탄 유전자 전달체 개발

August 2023

Seoul National University
Department of Agriculture, Forestry and Bioresources

Seoyoung Kim

Polyethylenimine-conjugated Arabinogalactan for Hepatocellular Carcinoma Targeted Gene Delivery Systems

Advised by Prof. Tae-il Kim

Submitting a master's thesis of Agriculture

June 2023

Seoul National University
Department of Agriculture, Forestry and Bioresources

Seoyoung Kim

Confirming the master's thesis written by
Seoyoung Kim
August 2023

Chair Seonyeong Kwak (Seal)

Vice Chair Tae-il Kim (Seal)

Examiner Ki Hoon Lee (Seal)

Abstract

Hepatocellular carcinoma (HCC) is the third leading cause of cancer-related deaths. Targeting asialoglycoprotein-receptor (ASGPR) which is overexpressed on hepatocytes is a promising strategy for delivering therapeutic agents for HCC treatments. In this study, polyethylenimine-conjugated arabinogalactan (AGP) was synthesized and suggested as a novel HCC-targeted gene delivery system. Applying the newly developed 'One-pot method', polyethylenimine (Mw 10,000 Da) was grafted to arabinogalactan in a controlled reaction. The Synthesis of AGPs was confirmed by ^{1}H NMR, FT-IR, and GPC. AGP 0.5X formed uniform sphere-shaped nanoparticles with smooth cationic surfaces and protected pDNA from degradation against serum proteins. The transfection efficiency of AGP 0.5X exceeded PEI25k at a weight ratio of 10 in HepG2 and exhibited superior intracellular trafficking behavior. Meanwhile, the ASGPR-active targeting ability of AGP 0.5X was proven by the dramatic reduction in transfection efficiency and cellular uptake when pre-treated with free galactose in ASGPR-overexpressed cells. When complexed with Bcl-2 siRNA, Bcl-2 mRNA expression was inhibited and apoptosis was induced. Therefore, AGP 0.5X is proposed as a potential HCC-targeted gene delivery carrier.

Keyword: Gene delivery systems, Arabinogalactan, Polyethylenimine, Hepatocellular carcinoma, Bcl-2 siRNA

Student Number : 2021-28034

Table of Contents

List of Table

List of Figures

Chapter 1. Introduction

Hepatocellular carcinoma (HCC), a type of primary liver cancer, is the third leading cause of cancer-related deaths worldwide [1-3]. HCC is one of the few cancers with an increasing incidence each year, highlighting the urgent need for the development of more effective and safer treatment modalities [4]. Therefore, various attempts including surgical resection, liver transplantation, radiofrequency ablation, and chemoembolization were made to provide an enhanced strategy for HCC treatment. Recently, targeted gene therapy with nanoparticles has gained attention for its ease of tailoring chemical/physical properties and reducing off-target side effects [5-6]. Nanocarriers such as polymeric nanoparticles, liposomes, and inorganic nanoparticles have been studied due to their nano-sized dimension for facile penetration, protection effect against degradation, or controlled release of drug molecules.

Asialoglycoprotein-receptor (ASGPR), uniquely overexpressed on hepatocytes, can be an attractive target for gene delivery systems. The major role of ASGPR is the clearance of glycoproteins in the bloodstream [7]. ASGPR binds to glycoproteins that contain terminal galactose, N-acetylgalactosamine, or glucose and facilitates internalization by clathrin-mediate endocytosis for further clearance. This indicates that biomolecules consisting of galactose, N-acetylgalactosamine, or glucose can be utilized as a ligand for ASGPR and applied as the targeting motif of gene delivery carriers.

Arabinogalactan is a natural polysaccharide widely known for its biocompatibility and water solubility [8]. The biosafety of Larch arabinogalactan has been approved by the U.S. Food and Drug Administration (FDA). Thus, arabinogalactan is commonly used in food industry and biomedical fields [9]. Although the monosaccharide composition and structure of arabinogalactan vary depending on the original source, it is generally known to be composed of over 80% of galactose [10]. This property makes arabinogalactan a potential biomaterial for HCC-targeted gene delivery carriers. However, the application of arabinogalactan as a gene carrier has not been reported so far. One possible explanation is that the unique branch structure of arabinogalactan makes it difficult to modify and functionalize. To functionalize arabinogalactan as a gene carrier, new chemistry appropriate for the branched structured arabinogalactan is needed.

This study proposes polyethylenimine-conjugated arabinogalactan (AGP) as a novel HCC-targeted gene system (**Figure 1**). Arabinogalactan was hypothesized to have an active targeting ability towards ASGPR while polyethylenimine (PEI) was expected to provide an endosome buffering effect and cationic properties. AGP was synthesized in a novel one-pot method which enabled controlled conjugation of arabinogalactan and PEI. AGP was complexed with Bcl-2 siRNA by electrostatic interaction (AGP/siRNA) and delivered to hepatocytes to evaluate the antitumor effects. AGP/siRNA can approach hepatocytes and undergo receptor-mediated endocytosis due to its ASGPR-active targeting ability. The proton sponge effect

of conjugated PEI enables AGP/siRNA to escape from the endosome efficiently. Released Bcl-2 siRNA binds to RNA-induced silencing complex (RISC) and cleaves Bcl-2 mRNA, resulting in Bcl-2 protein downregulation and apoptosis induction. Three different AGPs varying in PEI conjugation degree were synthesized and examined to find the optimal condition for hepatocyte-targeted gene delivery.

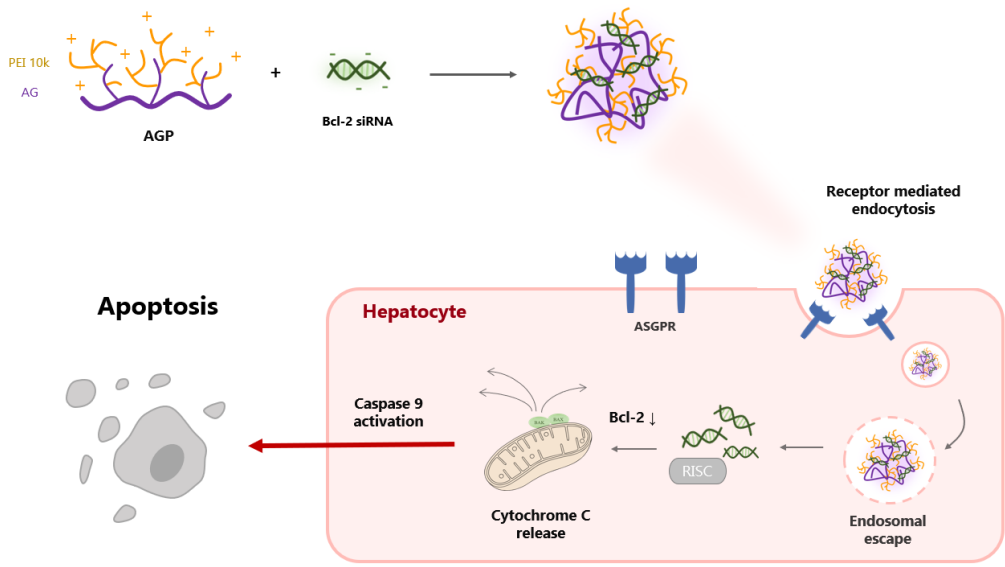

Figure 1. Schematic illustration of AGP/siRNA polyplex inducing apoptosis in hepatocyte.

Chapter 2. Literature Survey

2.1. Hepatocellular carcinoma targeted therapy

2.1.1. Asialoglycoprotein-receptor (ASGPR) targeted nanotherapy

The asialoglycoprotein receptor (ASGPR) is a C-type lectin that is primarily expressed on the sinusoidal surface hepatocytes. Targeting ASGPR can be a promising strategy for targeted receptor-mediated drug/gene delivery with minimum concerns of off-target side effects [7]. ASGPR exhibits a high affinity for carbohydrates specifically galactose, N-acetylgalactosamine, and glucose which can be utilized as targeting motifs in HCC-targeted treatments. [11]

Ahn et al. developed lysosome-targeting chimeras (LYTACs) that engaged the ASGPR as a lysosome-targeting receptor to degrade extracellular proteins in a cell-type manner. They conjugated binders to a triantenerrary N-acetylgalactosamine motif for targeting ASGPR to drive the downregulation of EGFR which contributes to HCC progression. [12] Ye et al. developed a methacrylate-based copolymer with galactose as ASGPR targeting moiety to deliver doxorubicin and Bcl-2 siRNA for HCC treatment. Successful codelivery of doxorubicin and Bcl-2 siRNA to the liver was proven in both subcutaneous and orthotopic HCC-bearing models [13]. Xu et al. developed self-activated cascade-responsive sorafenib and USP22 shNA co-delivery system for HCC treatment

using galactose fused lipopolyplex. Synergenic antitumor effect was observed in Huh-7 and BEL-7402. Also, the biodistribution and pharmacokinetics of the lipopolyplex confirmed HCC-targeting gene delivery in the HCC patient-derived xenograft model [14].

2.1.2. Arabinogalactan for drug delivery

Due to the high biocompatibility, excellent water-solubility, and the potential of targeting ASGPR, there have been attempts to utilize arabinogalactan as a drug delivery carrier for cancer treatments.

Pinhassi et al. developed arabinogalactan-folic acid-drug conjugate for the target-activated release of anticancer drugs to folate receptor-overexpressing cells [15]. The conjugate was synthesized by conjugating folic acid to arabinogalactan extracted from *Larix* tree and linking anticancer drugs to the folic acid. Arabinogalactan which was contributed as the template polymer, formed a stable nonvehicle. The conjugate exhibited high specificity to folate receptor-overexpressing cells. Targeted delivery and target-activated release of the anticancer drugs were successfully achieved.

Pathak et al. reported cholesterol-anchored arabinogalactan as a hepatospecific drug delivery system [16]. The conjugate was synthesized by covalently linking cholesterol to arabinogalactan, and further conjugating the model drug, ibuprofen, to cholesterol. The conjugate showed active targeting ability to the ASGPR and targeted delivery of ibuprofen to hepatocytes was successfully achieved *in*

vitro and *in vivo*.

2.2. Bcl-2 siRNA for tumor therapy

2.2.1. Role of Bcl-2 protein in cell apoptosis

Bcl-2 proteins are especially overexpressed in tumor cells, inhibiting cell death and contributing to the proliferation of tumors [17-18]. Apoptosis can be triggered by either extrinsic or intrinsic pathways. The extrinsic pathway includes cell surface receptors such as Fas and tumor necrosis factor receptor-1. The intrinsic pathway involves various genotoxic agents, metabolic insults, or transcriptional cues. BH3-only protein induction or post-translational activation initiates the intrinsic pathway by inactivating some Bcl-2 family members, thereby relieving the inhibition of BAX and BAK activation. The activation of BAX and BAK leads to mitochondrial fission and cytochrome c release, which activates APAF1 to form an apoptosome that activates caspase-9 and caspase-3. Caspases orchestrate the demolish the cells by cleaving a series of substrates and activating DNases. The extrinsic pathway can activate caspase-8 directly, which leads to caspase-3 activation and cell demolition, bypassing the mitochondrial step. The Bcl-2 family regulates the intrinsic pathway and can also modulate the extrinsic pathway through BID cleavage that communicates between the two pathways [19-20].

2.2.2. RNA interference with siRNA in tumor therapy

RNA interference (RNAi) is a phenomenon that silences gene expression and is utilized mostly in clinical and drug discovery fields [21]. RNAi can rapidly identify specific and potent inhibitors of disease targets from all molecular classes. Small interfering RNA (siRNA) is a type of genetic material that downregulates the expression of a specific protein. In the cytoplasm, siRNA binds to the RNA-induced silencing complex (RISC). Then, the RISC recognizes and cleaves complementary mRNA. The degradation of the target mRNA results in the inhibition of protein synthesis. siRNA is highly effective since it is activated outside the nucleus and has the advantage of being able to target specific sequences via complementary binding [22]. However, delivering siRNA itself exhibits low cellular uptake and is susceptible to nuclease-mediated degradation. Despite the high therapeutic potential of siRNA, its application in clinical settings is still limited mainly due to the lack of efficient delivery systems [23]. Thus, appropriate gene carriers that can protect and transport siRNA are needed.

2.3. Cationic polymer for gene delivery

2.3.1. Polyethylenimine (PEI) in gene delivery system

Polyethylenimine (PEI) is one of the widely used cationic polymers in non-viral gene delivery. Positively charged nitrogen atoms in PEI enable complexation with negatively charged molecules such as DNA

and induce efficient fusion with an anionic cellular membrane. These cationic properties make PEI an attractive material as a gene carrier [24]. Also, known as the “proton sponge effect”, unprotonated amines of PEI can absorb protons as they are pumped into the endosome, resulting in an increased influx of Cl^- ions and water molecules. This facilitates the rupture of endosomal membranes making PEI polyplex efficiently escape from the endosome [25].

2.3.2. PEI grafted polysaccharide for gene delivery

Despite the efficient gene-delivering ability of PEI, PEI with high molecular weight exhibit significant cytotoxicity. Therefore, modifications to reduce the potential toxicity of PEI are needed. One possible way is to conjugate PEI with biocompatible natural polymers.

Jiang et al. utilized dextran, a biodegradable natural polysaccharide, to reduce the toxicity of PEI and increase its stability in the presence of serum [26]. He et al. shielded the positive charge of PEI using hyaluronic acid to reduce cytotoxicity and prevent aggregation by salt and serum albumin [27]. To overcome low transfection efficiency driven by reduced electrostatic interaction of cell and conjugate, researchers developed a stimuli-responsive deshielding design.

Chapter 3. Materials and Methods

3.1. Materials

Arabinogalactan, branched polyethylenimine (PEI25k, 25 kDa), sodium chloride, heparin sodium salt from porcine intestinal mucosa, agarose, ethidium, bromide (EtBr), dimethyl sulfoxide (DMSO), ethanol, MicroBCA™ protein assay kit, 4',6-diamidono-2-phenylindole (DAPI), were purchased from Sigma-Aldrich (St. Louis, USA). Branched polyethylenimine (PEI10k, 10 kDa), sodium metaperiodate, D-galactose were purchased from Alfa-aesar (Ward Hill, USA). Sodium tetrahydroborate and HPLC water were purchased from Duksan (Ansan, Korea). Sodium hydroxide was purchased from Samchun (Gangnam, Korea). Dialysis membrane (MWCO 6-8 kDa) was purchased from SpectrumLABS (San Francisco, USA). Formic acid was purchased from Merck (Darmstadt, Germany). Polyethylene glycol was purchased in American polymer standards corporation (Blvd Mentor, USA). Triazolyl blue tetrazolium bromide (MTT) was purchased from GoldBio (St. Louis, USA). pDNA (pCN-Luci) was amplified by using Dyne DH5α Chemically Competent *E.Coli* ver.2 (DYNEBIO, Gangnam, Korea). NucleoBond® DNA extraction Xtra Maxi kit and Nucleospin RNA extraction kit were purchased from Macherey-Nagel (Düren, Germany). Dulbecco's Modified Eagle Medium (DMEM), and Minimal Essential Medium with Earle's Balanced Salts (MEM/EBSS) were purchased

from Cytiva (Gangnam, Korea). Dulbecco' s phosphate buffered saline (DPBS), DMEM GlutaMAX™ (GMX), fetal bovine serum (FBS), penicillin-streptomycin (P/S), and trypsin-EDTA were purchased from Gibco (New York, USA). Luciferase assay system and reporter lysis buffer were purchased from Promega (Madison, USA). Quant-iT™ PicoGreen™ dsDNA Assay kit, Alexa Fluor™ 488 Annexin V/Dead Cell Apoptosis Kit, YOYO-1 iodide, and Lysotracker™ Red DND-99 were purchased from Invitrogen (Waltham, USA). PrimeScript™ RT Reagent Kit (Perfect Real Time) and TB Green® Premix Ex Taq™ II (Tli RNaseH Plus) were purchased from TaKaRa (Kusatsu, Japan). Bcl-2 siRNA (5'-GUGAAGUCAACAUGCCUGC-3' (sense), 5'-GCAGGCAUGUUGACUUCAC-3' (antisense)), Bcl-2 primer, GAPDH primers listed in Table 1 were purchased from Bioneer (Daejeon, Korea)

Table 1. Primer sequences used in qPCR.

	Sequence (5' → 3')	Ref
Bcl-2 primer (forward)	5'-GGATTGTGGCCTTCTTTGAG-3'	[28-29]
Bcl-2 primer (reverse)	5'-CCAAACTGAGCAGAGTCTTC-3'	
GAPDH primer (forward)	5'-TCAACGGCACAGTCAAGG-3'	[30]
GAPDH primer (reverse)	5'-ACTCCACGACATACTCAGC-3'	

3.2. Methods

3.2.1. Synthesis of AGP

3.2.1.1. Structure analysis of arabinogalactan

To determine the linkage type of arabinogalactan, ^{13}C NMR (600 MHz, AVANCE 600, Brucker, Germany) analysis was conducted. The sample was prepared by dissolving in D_2O at a concentration of 50 mg/mL.

3.2.1.2. Synthesis of AGP

To synthesize AGP, arabinogalactan and PEI (Mw 10,000 Da) were dissolved in ultra-pure water and stirred continuously at room temperature. The amount of PEI mixed was 5-fold molar excess of vicinal diols in arabinogalactan. Three different amounts of sodium metaperiodate (0.2, 0.5, 1-fold molar excess relative to the vicinal diols of arabinogalactan) were added dropwise to oxidize vicinal diols to aldehyde groups. After 24 h of reaction at 25℃, an excessive amount of sodium tetraborohydrate was added and the solution was continuously stirred overnight. The solutions were dialyzed against ultra-pure water for 72 h using a dialysis membrane (MWCO: 6-8 kDa) and freeze-dried for 72 h. Finally, three products with different degrees of conjugation were obtained and named as AGP 0.2X, 0.5X, and 1X according to the amount of periodate added.

3.2.2. Characterization of AGP and AGP/pDNA polyplex

3.2.2.1. Structural analysis of AGP

The conjugation of arabinogalactan and PEI was confirmed by ^{1}H NMR (600 MHz, AVANCE 600, Brucker, Germany). Each sample was prepared in D_2O at a concentration of 10 mg/mL. The structure of AGP was further analyzed by Fourier transforms infrared (FT-IR) spectroscopy. Attenuated total reflectance (ATR) FTIR spectroscopy (Nicolet 6700, Thermo Scientific, USA) was used. Each spectrum was obtained with resolution of 8 cm^{-1} and 32 scans in the wavenumber range of 3100-650 cm^{-1}.

The purification process was confirmed by gel permeation chromatography (GPC, YL-9100 HPLC System, Youngin Chomass, Korea) with Ultrahydrogel 250 column (Waters, USA). Poly(ethylene glycol)s with various molecular weights were used as standards for the analysis and 1% formic acid was used as the solvent. AGPs were dissolved in the solvent at a concentration of 10 mg/mL and analyzed at 0.6 mL/min of flow rate.

3.2.2.2. Endosome buffering capacity measurement

To examine the endosome buffering capacities of AGPs acid-based titration was performed. 5 mg of polymer was dissolved in 5 mL of 0.1 M aqueous NaCl solution and adjusted to pH 11 using 1 M NaOH. Then, the solutions were titrated to pH 2.5 with 0.1 M HCl. pH changes of the solution were measured by pH meter (SevenEasy pH meter S20, Mettler-Toledo, Columbus, OH, USA). Endosome

buffering capacity was calculated as a percentage of amine groups becoming protonated within the pH range from 7.4 to 5.1, according to the following equation.

$$\text{Buffering capacity (\%)} = \frac{\Delta V(HCl) \times 0.1\ M}{N\ mol} \times 100\ (\%)$$

where ΔV(HCl) is the volume of HCl solution added to change the pH value of the polymer solution from 7.4 to 5.1. N mol is the total moles of protonable amine groups in 5 mg of each polymer.

3.2.2.3. pDNA condensing ability assessment

To evaluate pDNA condensing ability of AGP, agarose gel retardation assay was conducted. AGP and pDNA were mixed at various weight ratios (polymer/pDNA, w/w) ranging from 0.1 to 1 in HEPES buffer (pH 7.4). After 30 min of incubation at room temperature, samples were loaded on agarose gel (0.7%, w/v) containing EtBr solution (0.5 μg/mL). Samples were electrophoresed at 90 V for 12 min using Mupid-2plus® (OPTIMA, Japan). pDNA bands were visualized using GelDoc™ XRS+ gel documentation system (BIO-RAD, USA).

pDNA condensing ability was further examined by PicoGreen assay using Quant-iT™ PicoGreen™ dsDNA Assay kit (Invitrogen, USA). The polymers and pDNA were mixed at various weight ratios ranging from 0.1 to 1 in Tris-EDTA (TE) buffer (0.5 μg pDNA). After 30 min of incubation at room temperature, 100 μL of polyplex solutions

were loaded in 96-well black plate. Then, 100 μL of PicoGreen reagent solutions were added to each well and incubated for 4 min in dark conditions. The fluorescence (Ex: 480 nm, Em: 520 nm, sensitivity: 50) of each sample was measured using a microplate reader (Synergy H1, BioTek, USA). The results were presented as relative fluorescence (%, fluorescence of sample/fluorescence of free pDNA). All the measurements were performed three times.

3.2.2.4. Average size and zeta-potential measurement

The average size and zeta-potential values of AGP/pDNA polyplex were measured by Zetasizer (Nano ZS90, Malvern Instruments, UK). Polyplex solutions were prepared in ultra-pure water at various weight ratios ranging from 0.1 to 100. After 30 min of incubation at room temperature, measurement was processed. All the measurements were performed three times.

3.2.2.5. Morphology of AGP/pDNA polyplex

The morphology of AGP/DNA polyplexes (weight ratio 10) was observed with energy-filtering transmission electron microscope (EF-TEM, LIBRA 120, Carl Zeiss, Germany). 10 μL of AGP/pDNA polyplex were loaded on copper carbon film 300 mesh (CF300-Cu-50, Electron microscopy science, USA) for 1 min. After blotting the grid with filter paper, 5 s of 2% uranyl acetate staining was followed. After absorbing the residual solutions, the images were visualized with an accelerating voltage of 120 kV.

3.2.2.6. Heparin competition assay

Various weight ratios of AGP/pDNA polyplexes were prepared in HEPES buffer (pH 7.4) for 30 min at room temperature. Then, 2 μL of various concentrations of heparin solution were added to each sample and gently mixed 5 times. The samples were then incubated at 37℃ for an additional 30 min. Subsequently, the samples were loaded on agarose gel (0.7% w/v) containing EtBr solution (0.5 μg/mL) and electrophoresed for 12 min at 90 V using Mupid-2plus® (OPTIMA, Japan). pDNA bands were visualized using GelDoc™ XRS+ gel documentation system (BIO-RAD, USA).

3.2.2.7. pDNA protection from serum protein

Various weight ratios of AGP/pDNA polyplexes were prepared under 50% FBS and 2 μL heparin solution (4 mg/mL) for 30 min at 37℃. Subsequently, the samples were loaded on agarose gel (0.7% w/v) containing EtBr solution (0.5 μg/mL) and electrophoresed for 12 min at 90 V using Mupid-2plus® (OPTIMA, Japan). pDNA bands were visualized using GelDoc™ XRS+ gel documentation system (BIO-RAD, USA).

3.2.3. *In vitro* assay of AGP and AGP/pDNA polyplex

3.2.3.1. Cell culture

Human HCC cell lines HepG2, Hep3B, and human cervical adenocarcinoma cell line HeLa were used for *in vitro* experiments. Cells were cultured in a medium containing 10% FBS and 1% penicillin/streptomycin. DMEM, MEM/EBSS, and DMEM GlutaMAX™ were used as the medium for HepG2, Hep3B, and HeLa cells respectively. All cells were maintained in 5% CO_2 incubator at 37℃.

3.2.3.2. Cytotoxicity of AGP

To analyze the cytotoxicity of AGPs, MTT assay was performed on HepG2, Hep3B, and HeLa cell lines. The cells were seeded on a 96-well cell culture plate at a density of 1×10^4 cells/well. After 24 h of incubation and achieving 70—80% confluency, 100 μL of polymer solutions (serum-free medium) with various concentrations were treated in each well for 4 h. Then, the media was changed to a fresh medium (10% FBS). After another 24 h incubation, 25 μL of MTT solution (2 mg/mL in DPBS) was added to each well and incubated for 2 h at 37℃. The medium was removed and 150 μL of DMSO was added to each well to dissolve the formazan crystal. The absorbance was measured at 570 nm using a microplate reader (Synergy H1, BioTek, USA). The results were presented as relative cell viability (RCV, percentage values relative to value of untreated cells).

3.2.3.3. Luciferase transgene expression assay

The transfection efficiency of AGP was analyzed via luciferase transgene expression assay [31]. After cell incubation, the media were exchanged with 400 μL of serum-free medium for the assay in non-serum condition and serum-containing medium (10% FBS) for the assay in serum condition. In the case of galactose competition, prior to media exchange, free galactose (1 mM, serum-containing media) was pre-treated for 30 min at 37℃. Then, 100 μL of AGP/pDNA polyplex solutions (0.5 μg pDNA, serum-free medium) with various weight ratios were treated. PEI25k/pDNA polyplex at a weight ratio of 1 was used as the control. After 4 h of incubation at 37℃, the medium was changed to fresh medium (10% FBS) and further incubated for 48 h. Subsequently, media were removed and each well was rinsed with DPBS twice. Then, cells in each well were lysed with 120 μL of Reporter lysis buffer for 2 h and centrifuged (14000 rpm, 10 min, 4℃) to spin down the lysate.

20 μL of supernatants for each sample were loaded in a white 96-well plate, and luminescence was measured after adding 100 μL of luciferase assay buffer. Meanwhile, a protein quantification assay was conducted to measure the total amount of cellular proteins. 20 μL of supernatant were mixed with 130 μL of ultra-pure water and 150 μL of BCA reagent provided in MicroBCA™ protein assay kit. After 2 h of incubation at 37℃, the absorbance was measured at 562 nm. The results were presented in relative luminescence unit per unit mg of cellular protein (RLU/mg protein). The luminescence and the

absorbance of the sample were both measured by a microplate reader.

3.2.3.4. Cellular Uptake

The cellular uptake of AGP/pDNA polyplex was analyzed by flow cytometry. Cells were seeded on a 6-well cell culture plate at a density of 2×10^5 cells/well. After 24 h of incubation and achieving 70—80% confluency, the media were exchanged with 1.5 mL of serum-free medium. In the case of galactose competition, prior to media exchange, free galactose (1 mM, serum-containing media) was pre-treated for 30 min at 37℃. Then, 500 μL of AGP/pDNA polyplex solution (2 μg pDNA, serum-free medium), in which pDNA is labeled with YOYO-1 iodide (1 molecule of the dye per 50 base pairs of the nucleotide) was treated. After 4 h of treatment at 37℃, the medium was removed and each well was rinsed with ice-cold DPBS twice. Following trypsinization, cells were resuspended in 1 mL of DPBS. The cellular uptake of fluorescence-labeled polyplexes was measured by BD Accuri C6 flow cytometer (BD Biosciences, USA) at a minimum of 1×10^4 cells gated per sample. The top 0.5% fluorescent signals of untreated cells were considered as successful cellular uptake. Analysis was performed by BD Accuri C6 software.

3.2.3.5. Intracellular trafficking visualization

Confocal laser scanning microscope (CLSM, SP8 X STED, Leica, Wetzlar, Germany) was used to observe the intracellular trafficking of the polyplex. HepG2 cells were seeded on a confocal dish at a density of 1×10^5 cells/well and incubated at 37℃ for 24 h to reach 70—80% of confluency. AGP/pDNA polyplex was prepared at a weight ratio of 10, where pDNA was labeled with YOYO-1 iodide. The polyplex solution (1 μg pDNA/dish, serum-free medium) was treated for 2, 4, and 8 h. In the case of the 8 h treatment, the medium was changed to fresh media (10% FBS) after 4 h of treatment and further incubated for 4 h. Same process was done for PEI25k/pDNA polyplex at a weight ratio of 1. Upon completion of the predetermined incubation time for all samples, acidic organelles were stained with Lysotracker Red DND-99 solution (200 nM) for 30 min. Then, cells were fixed with 4% paraformaldehyde for 10 min. Finally, nuclei were stained with DAPI solution (0.125 μg/mL) for 10 min. Following sufficient rinsing with DPBS, polyplex and cells were visualized with CLSM. The obtained images were processed with LAS X software. Pearson's coefficient was calculated by using JACop imageJ to describe the colocalization of two different fluorescence signals.

3.2.4. Antitumor effect of AGP/siRNA

3.2.4.1. Characterization of AGP/siRNA

AGP and Bcl-2 siRNA were mixed in ultra-pure water at a weight ratio of 10 and incubated for 30 min at room temperature. Then, the average size and zeta-potential of AGP/siRNA were measured by Zetasizer. All the measurements were performed three times.

3.2.4.2. Bcl-2 silencing effect

Bcl-2 mRNA expression level was analyzed via Quantitative real-time polymerase chain reaction (RT-qPCR). HepG2 cells were seeded on a 6-well cell culture plate at a density of 2×10^5 cells/well. After 24 h of incubation and achieving 70—80% confluency, the media were exchanged to 1.5 mL of serum-free medium. Then, 500 μL of free Bcl-2 siRNA, PEI/siRNA, AGP/siRNA solution (2 μg Bcl-2 siRNA, serum-free medium) were treated to each well. The weight ratio of PEI/siRNA and AGP/siRNA were fixed to 1 and 10, respectively. After 4 h of treatment at 37℃, media was exchanged to fresh media (10% FBS) and cells were further incubated for 48 h.

RNA extraction was performed using Nucleospin RNA extraction kit (Macherey-Nagel, Germany). Cells were harvested by trypsinization and RNA was isolated according to the manufacturer's protocol. The concentration of extracted RNA was measured by Take 3 microvolume plate (Synergy H1, BioTek, USA). Extracted RNA was reverse transcribed into cDNA using PrimeScript^{TM} RT Reagent Kit (TaKaRa, Japan). RT-qPCR was performed using SYBR Premix

Ex Taq II kit (TaKaRa, Japan) and a real-time PCR machine (Applied Biosystems, USA). The samples were run at 95℃ for 30 s for denaturation and followed by 45 cycles of PCR, which consisted of denaturation (95℃, 5 s), annealing (55℃, 30 s), and polymerization (72℃, 30 s). The expression levels of target genes were normalized using GAPDH and the $2^{-\Delta\Delta CT}$ method.

3.2.4.3. Antitumor effect analysis with MTT assay

To investigate the antitumor effect on HCC, MTT assay was conducted on HepG2 cells. HepG2 cells were seeded on a 96-well cell culture plate at a density of 1×10^4 cells/well. After 24 h of incubation and achieving 70—80% confluency, 100 μL of free Bcl-2 siRNA, PEI/siRNA, AGP/siRNA solution (0.1 μg Bcl-2 siRNA/well, serum-free medium) were treated for 4 h. The weight ratio of PEI/siRNA and AGP/siRNA were fixed to 1 and 10, respectively. Then, the media was changed to a fresh medium (10% FBS). After another 24 h incubation, 25 μL of MTT solution (2 mg/mL in DPBS) was added to each well and incubated for 2 h at 37℃. The medium was removed and 150 μL of DMSO was added to each well to dissolve the formazan crystal. The absorbance was measured at 570 nm using a microplate reader. The results were presented as relative cell viability (RCV, percentage values relative to value of untreated cells).

3.2.4.4. Apoptosis induction test with Annexin V staining

Apoptosis induction was analyzed by Annexin V staining using Alexa Fluor™ 488 Annexin V/Dead Cell Apoptosis Kit (Invitrogen, USA). HepG2 cells were seeded on a 6-well cell culture plate at a density of 2×10^5 cells/well. After 24 h of incubation and achieving 70—80% confluency, the media were exchanged with 1.5 mL of serum-free medium. Then, 500 μL of AGP/siRNA solution (2 μg Bcl-2 siRNA/well, serum-free medium) was treated. After 4 h of treatment at 37℃, media was exchanged to fresh media (10% FBS) and cells were further incubated for 48 h. The cells were rinsed with DPBS twice and harvested by trypsinization. Detached cells were resuspended in 100 μL of Annexin binding buffer, and stained by Alexa fluor 488 and propidium iodide (PI) for 15 min at 25℃. After adding 400 μL of annexin binding buffer, all samples were kept in ice and analyzed by BD Accuri C6 flow cytometer with BD Accuri C6 software.

Chapter 4. Results and Discussion

4.1. Synthesis of AGP

4.1.1. Structural analysis of arabinogalactan

The composition and structure of natural polysaccharides differ depending on their sources. In this study, arabinogalactan extracted from larch wood was used as the main material. To identify its specific linkage types and monosaccharide composition, ^{13}C NMR spectra were analyzed (**Figure 2**). Carbon peaks of arabinogalactan were assigned based on the results of several literatures [10, 32]. NMR spectra revealed that the arabinogalactan backbone consisted of a backbone of β−1,3−linked galactose and branches of β−1,6−linked galactose or arabinose at C6. The composition ratio of galactose and arabinose was found to be 6.08: 1, which corresponds to the previous reports of larch arabinogalactan [10].

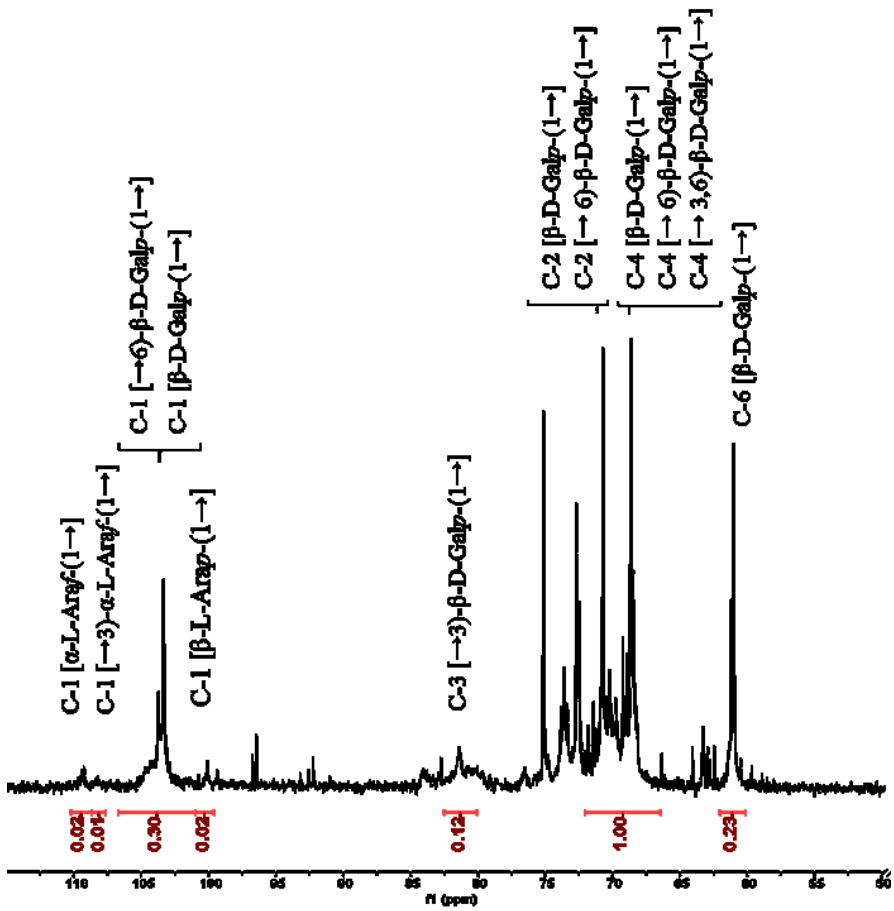

Figure 2. ^{13}C NMR spectra of arabinogalactan.

Table 2. Linkage type and composition ratio of arabinogalactan.

Linkage type		Composition ratio	Sum
Backbone	β-D-Gal*p* (1 → 3)	13	33
	β-D-Gal*p* (1 → 3,6)	20	
Branch	β-D-Gal*p* (1 → 6)	20	52
	β-D-Gal*p* (1 →	20	
	α-L-Ara-(1→	4	
	β-L-Ara-(1→	4	
	α-L-Ara-(1→3)	4	

4.1.2. Synthesis of AGP

AGP 0.2X, 0.5X, and 1X were synthesized via “One pot method”, a novel conjugation method. In previous studies, PEI–polysaccharide conjugation was processed in two steps. In brief, the first step is to obtain an oxidized polysaccharide using periodate, which serves as an intermediate product. The sond step is to dissolve the oxidized polysaccharide in a new solvent and react it with primary amines of PEI. However, when AGP was synthesized following the method, excessive crosslinking occurred, producing insoluble products and nano–aggregates.

The reason for the uncontrolled reaction is due to the unique branched structure of arabinogalactan. As mentioned above, arabinogalactan is composed of a β–1,3–linked galactose backbone and branches with β–1,6–linked galactose or arabinose at C6. Therefore, all vicinal diols are located on branches which makes them highly accessible to other functional groups. When oxidized arabinogalactan reacts with branched PEI, excessive crosslinking occurs between two multifunctional polymers and results in insoluble products. Meanwhile, conjugation with PEI occurs only at one side of the polymer, resulting in partially hydrophilic relative to the backbone. Hence, the hydrophobic interaction of the backbone induces nano–aggregation of AGPs in an aqueous solution.

The newly developed One–pot method prevents excessive crosslinking by adding a small amount of periodate *in situ*, which allows the partial formation of aldehyde groups. Furthermore, by

stirring arabinogalactan and PEI together, the partially formed aldehyde groups can immediately form Schiff bases with the primary amines of PEI. Applying this novel method, AGP was obtained via mild and controlled conjugation. AGP exhibited excellent water solubility with no aggregation. Also, the One-pot method has the advantage of simplifying the conjugation step and significantly shortening the synthesis period.

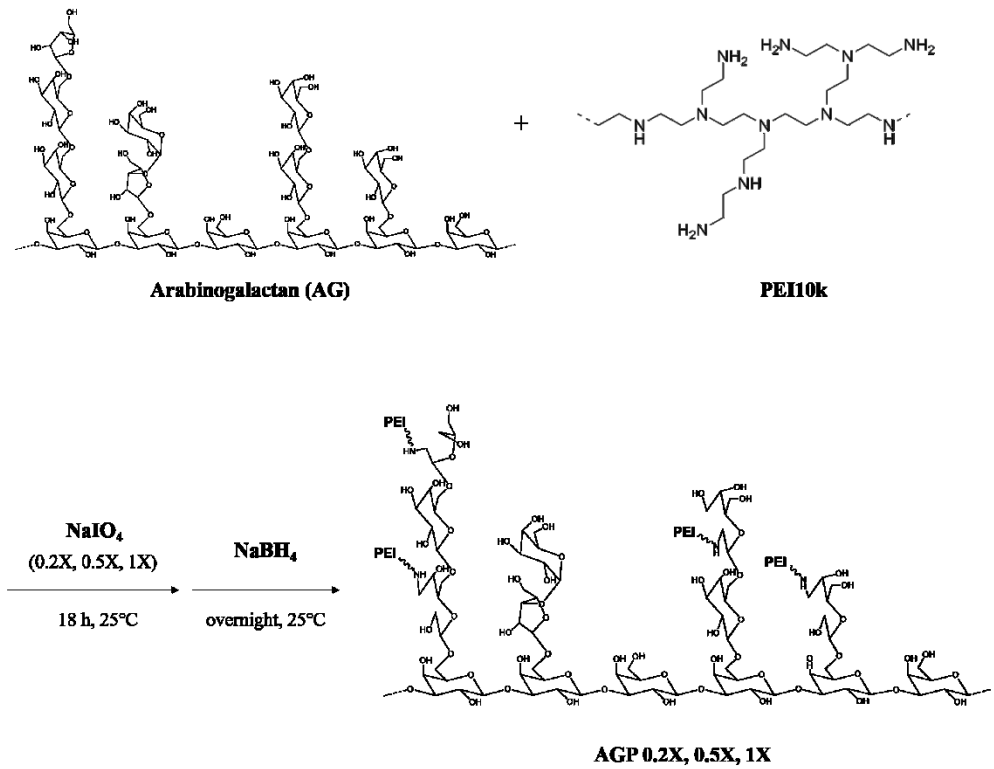

Figure 3. One-pot synthesis of AGP.

4.2. Characterization of AGP and AGP/pDNA polyplex

4.2.1. Structural analysis of AGP

Structural analysis of AGP 0.2X, 0.5X, and 1X was performed by ^{1}H NMR (**Figure 4**). Proton peaks of arabinogalactan and PEI were observed at δ 3.120–4.597 and δ 2.131–3.120, respectively. The increase in PEI peak area with an increase in oxidation degree demonstrates the controlled synthesis of AGP. Assuming that the repeating unit of arabinogalactan is composed of 6.08 galactose and one arabinose, AGP 0.2X, 0.5X, and 1X were conjugated with 0.13, 0.34, 0.69 PEI10k per arabinogalactan unit, respectively.

The synthesis of AGP was further confirmed by FT-IR measurement (**Figure 5**). N-H peaks (3100–2800 cm^{-1}, 1650–1580 cm^{-1}) which were absent in arabinogalactan, were observed in AGPs. C-N peaks (1250–1020 cm^{-1}) were found in AGPs describing that covalent bonds between arabinogalactan and PEI were successfully formed. Moreover, the complete removal of unreacted materials was confirmed by GPC measurement. As shown in **Figure 6**, all three samples (AGP 0.2X, 0.5X, and 1X) showed a single peak, indicating successful synthesis and purification. In addition, the weight average molecular weight (Mw) of all samples were in the range of 30–33 kDa.

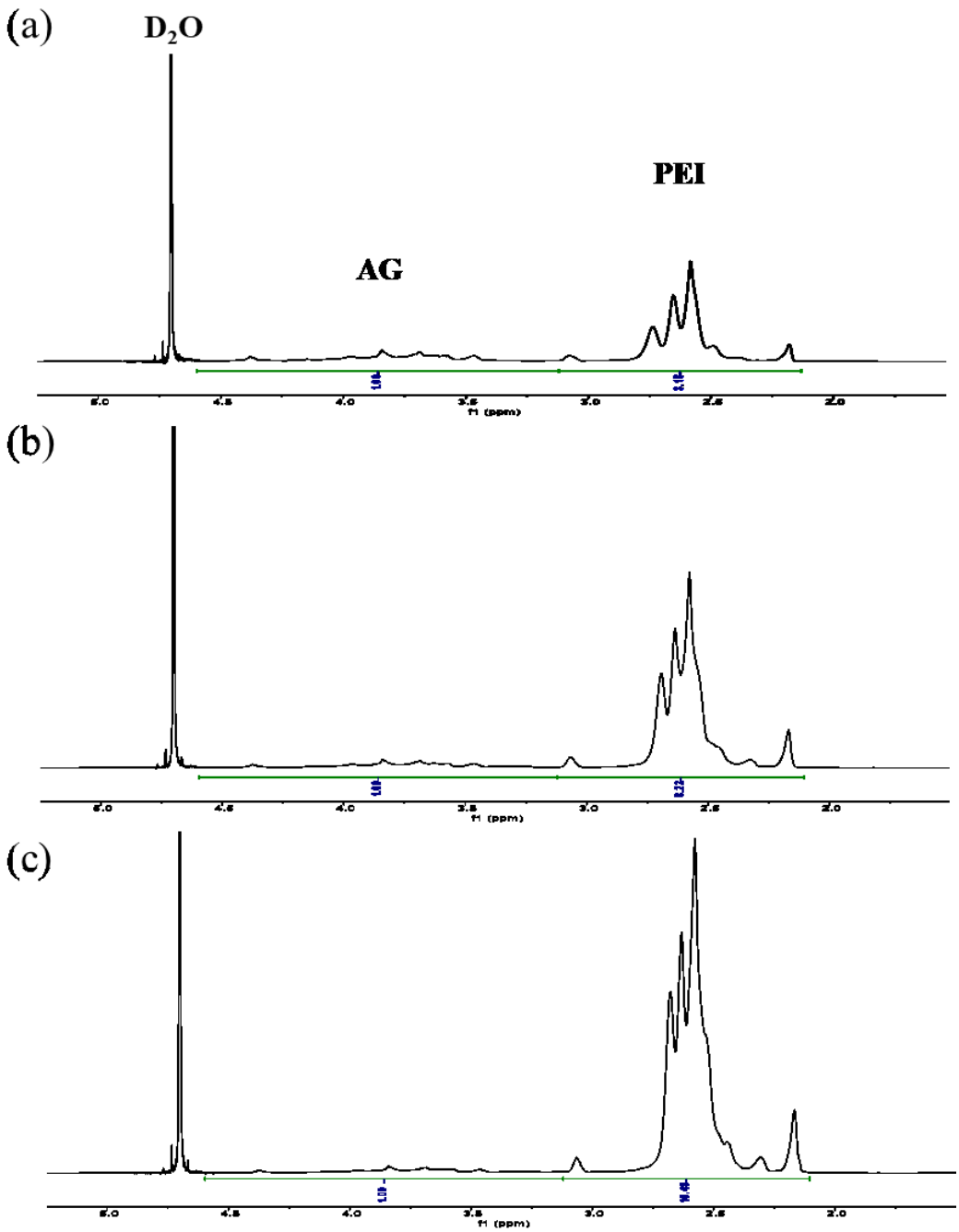

Figure 4. ^{1}H NMR spectra of (a) AGP 0.2X, (b) AGP 0.5X, and (c) AGP 1X.

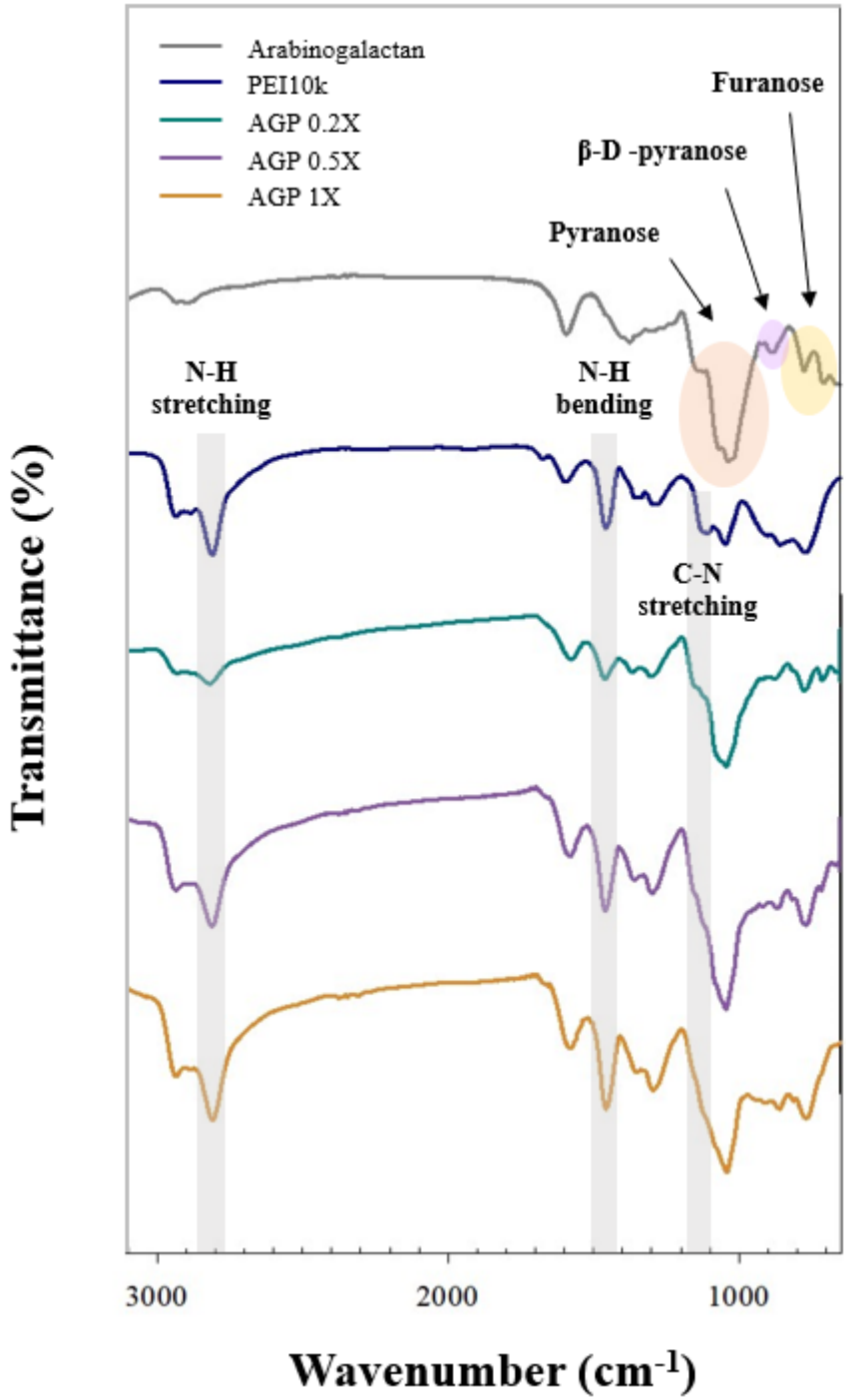

Figure 5. FT-IR spectra of arabinogalactan, PEI10k, AGP 0.2X, AGP 0.5X, and AGP 1X.

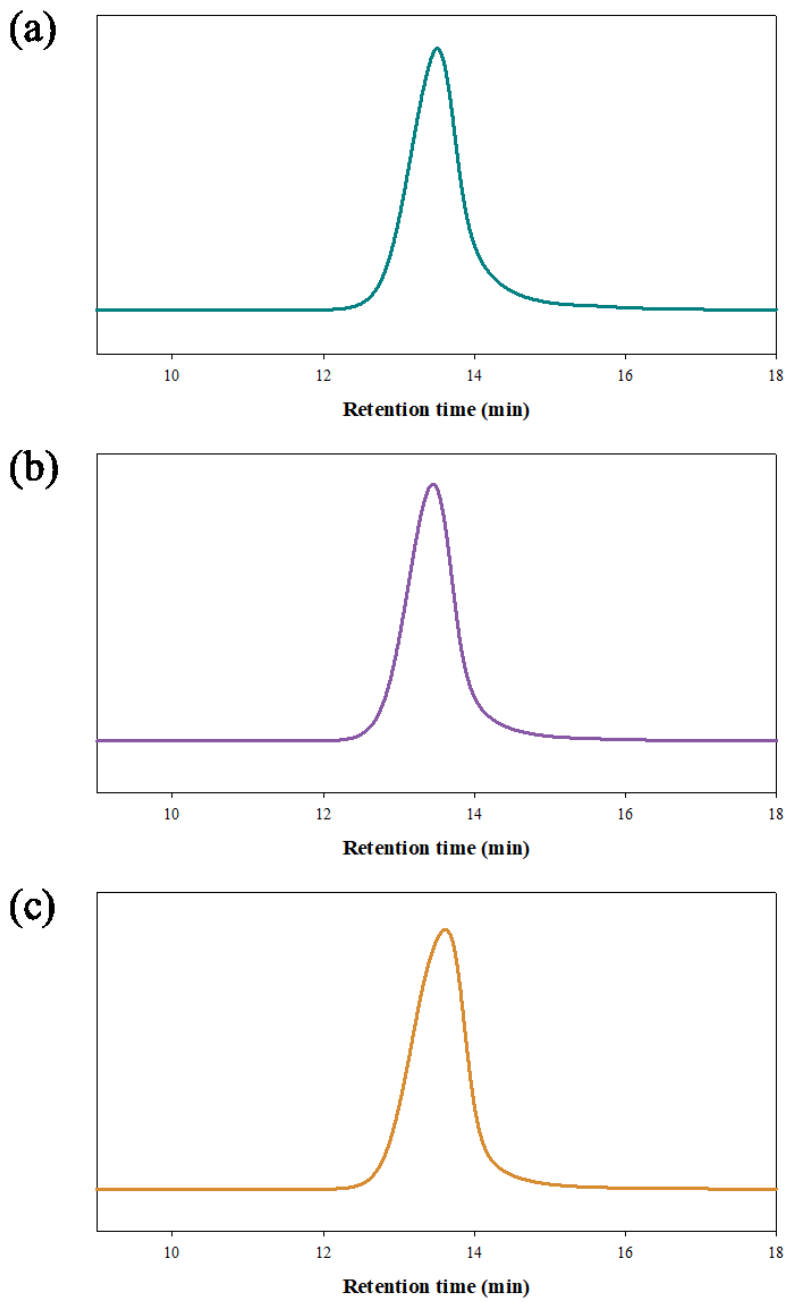

Figure 6. GPC chromatograms of (a) AGP 0.2X, (b) AGP 0.5X, and (c) AGP 1X. 1% formic acid was used as the solvent.

4.2.2. Endosome buffering capacity measurement

In polymeric drug/gene delivery, high endosome buffering capacity leads to efficient endosomal escape which enables enhanced drug/gene delivery [32-34]. Therefore, the endosome buffering capacity of AGPs was examined via acid-base titration (**Figure 7**, **Table 3**) [35].

Based on the conjugation ratio calculated from ^{1}H NMR spectra, molecular weights of AGP 0.2X, 0.5X, and 1X were determined and approximate buffering capacity was calculated. According to ^{1}H NMR spectra, the calculated buffering capacity for AGP 0.2X, 0.5X, and 1X were 15.71%, 16.71%, and 21.49%, respectively. Meanwhile, the buffering capacity of PEI25k was 18.10%. Thus, it is indicated that AGPs exhibit similar buffering capacity to PEI25k.

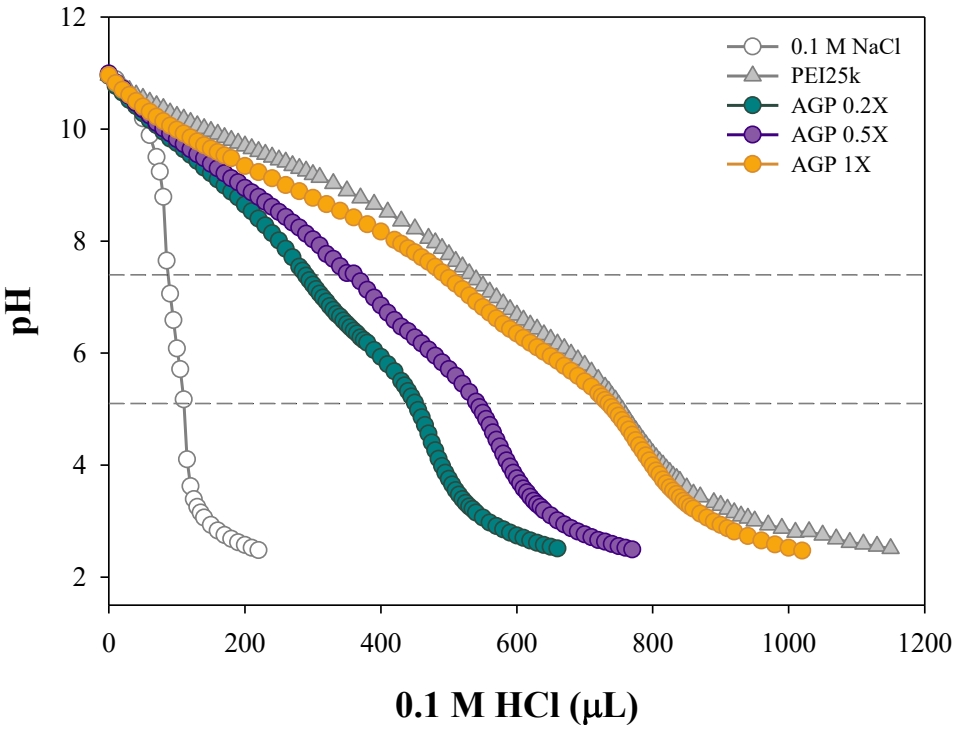

Figure 7. Acid–base titration curve of PEI25k, AGP 0.2X, AGP 0.5X, and AGP 1X. 5 mg of each polymer was dissolved in 5 mL of 0.1 M NaCl solution. Dashed lines depict the endosomal pH range (5.1 and 7.4).

Table 3. Buffering capacity of PEI25k, AGP 0.2X, AGP 0.5X, and AGP 1X.

	PEI25k	AGP 0.2X	AGP 0.5X	AGP 1X
Buffering Capacity (%)	18.10	15.71	16.71	21.49

4.2.3. pDNA condensing ability assessment

Agarose gel electrophoresis was performed to investigate pDNA condensing ability of AGPs. Cationic AGP can be complexed with negatively charged pDNA through electrostatic interaction [36]. As shown in **Figure 8**, AGP 0.2X retarded pDNA completely at a weight ratio of 1 while AGP 0.5X and AGP 1X condensed pDNA at a weight ratio of 0.7 and 0.5, respectively. pDNA condensing ability of AGP enhanced with the increase in the grafted amount of PEI.

pDNA complexation ability of AGP was further proved by PicoGreen assay (**Figure 9**). PicoGreen reagent is a fluorescent dye molecule that emits fluorescence when it is bound to dsDNA, enabling the quantification of DNA. The fluorescence value of the PicoGreen reagent decreased with the increase in the weight ratio of AGP/pDNA polyplex. This indicates that AGP hindered the intercalation of the PicoGreen reagent into pDNA by compactly condensing pDNA.

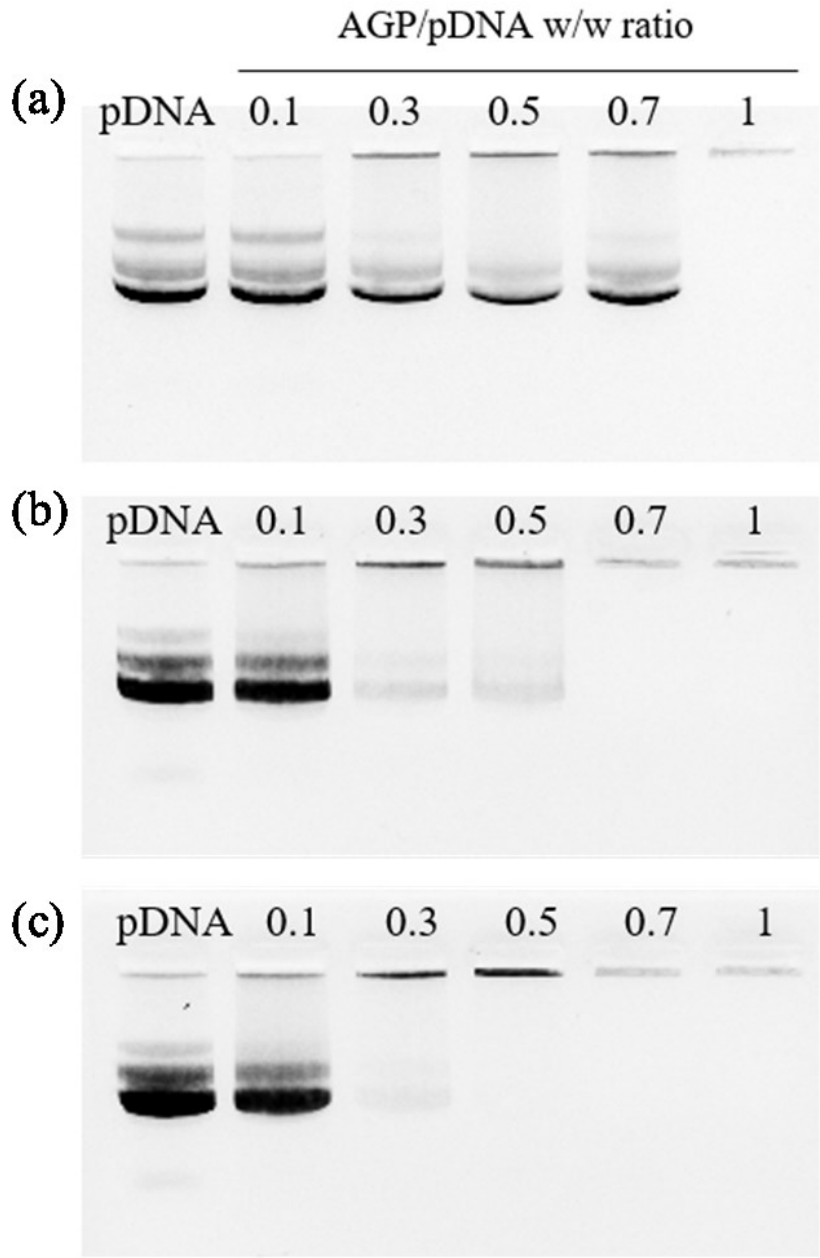

Figure 8. Agarose gel electrophoresis results of (a) AGP 0.2X/pDNA, (b) AGP 0.5X/pDNA, and (c) AGP 1X/pDNA polyplexes at various weight ratios.

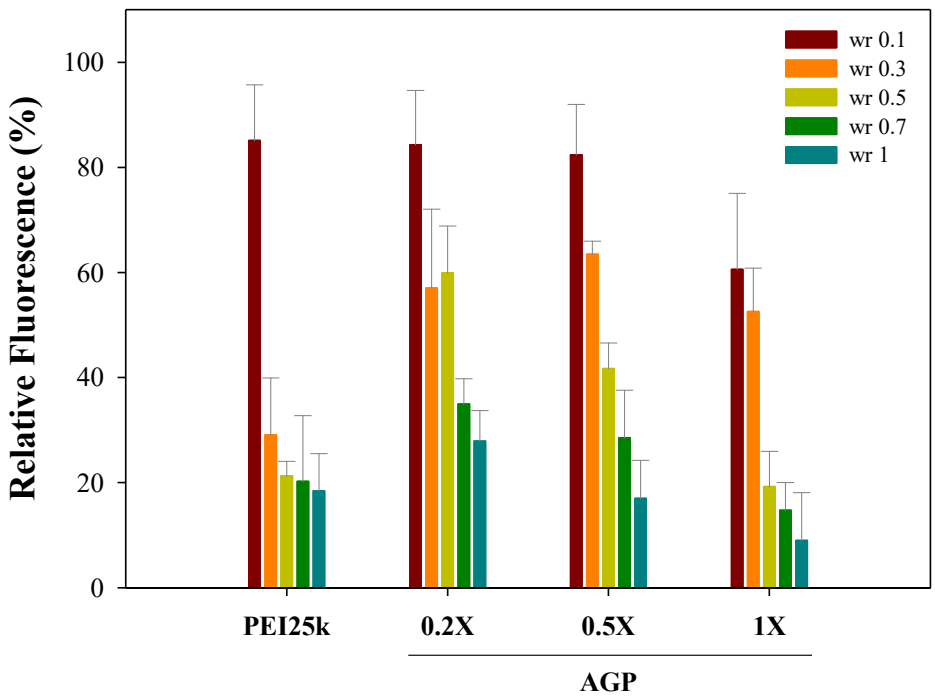

Figure 9. PicoGreen assay result of PEI25k, AGP 0.2X, AGP 0.5X, and AGP 1X polyplexes at various weight ratios.

4.2.4. Average size and zeta-potential measurement

Enhanced cellular uptake and circulation time of nanoparticles can be achieved by tailoring the size and surface properties. It is known that nanoparticles under 100-200 nm in diameter are internalized via clathrin-mediated endocytosis (CME), while larger nanoparticles up to 500 nm, are internalized by caveolae-mediated endocytosis (CVME) [37-38]. Many studies have proved that receptor-mediated endocytosis occurs through the mechanism of CME. Thus, the optimal size range of nanoparticles is 100-200 nm to induce cellular uptake through the ASGPR [39]. Also, the cationic surface charge of the nanoparticle drives affinity to the negatively charged cellular membrane, enhancing cellular uptake [40]. Moreover, positively charged nanoparticles are more easily taken up via CME while negatively charged nanoparticles are more likely to enter to cell through CVME [41]. Therefore, the Z-average size and zeta-potential value of AGP/pDNA polyplexes were measured at various weight ratios (**Figure 10**).

AGP/pDNA polyplexes showed a consistent size of 140-250 nm from a weight ratio of 10. At a weight ratio of 10, AGP 0.2X, 0.5X, and 1X formed polyplexes of 150±8.70 nm, 195.63±3.21 nm, and 197.33±8.17 nm, respectively. Zeta-potential value of AGP/pDNA polyplexes was converted from a negative value to a positive value at a specific weight ratio. Charge conversion occurred at a weight ratio of 1 in AGP0.2X and AGP 0.5X. AGP 1X showed a positive value at a lower weight ratio (0.5), due to more conjugation of cationic PEI.

At a weight ratio of 10, AGP 0.2X, 0.5X, and 1X formed polyplexes of 33.63±0.94 mV, 42.27±0.43 mV, and 44.53±0.07 mV, respectively. This result indicates that AGP could form positively charged polyplexes with pDNA at low weight ratios. Moreover, polyplexes at a weight ratio of 10 possess physicochemical conditions suitable for receptor-mediated endocytosis.

4.2.5. Morphology of AGP/pDNA polyplex

The morphology of the AGP/pDNA polyplexes was observed using TEM (**Figure 11**). All polyplexes were formed at a weight ratio of 10. AGP 0.2X/pDNA polyplex was non-uniformly shaped while AGP 0.5X and AGP 1X formed uniformly spherical particles. In the case of AGP 0.5X/pDNA polyplex, the surface density was higher than the internal density, which resulted in the smooth edge of the polyplex. On the other hand, the edge of AGP 1X/pDNA polyplex was relatively rough which indicates that the internal density was higher than the surface density. The flexibility and structural properties of polymer may have affected the difference in density. However, further studies are needed to verify the morphological characteristics of AGPs.

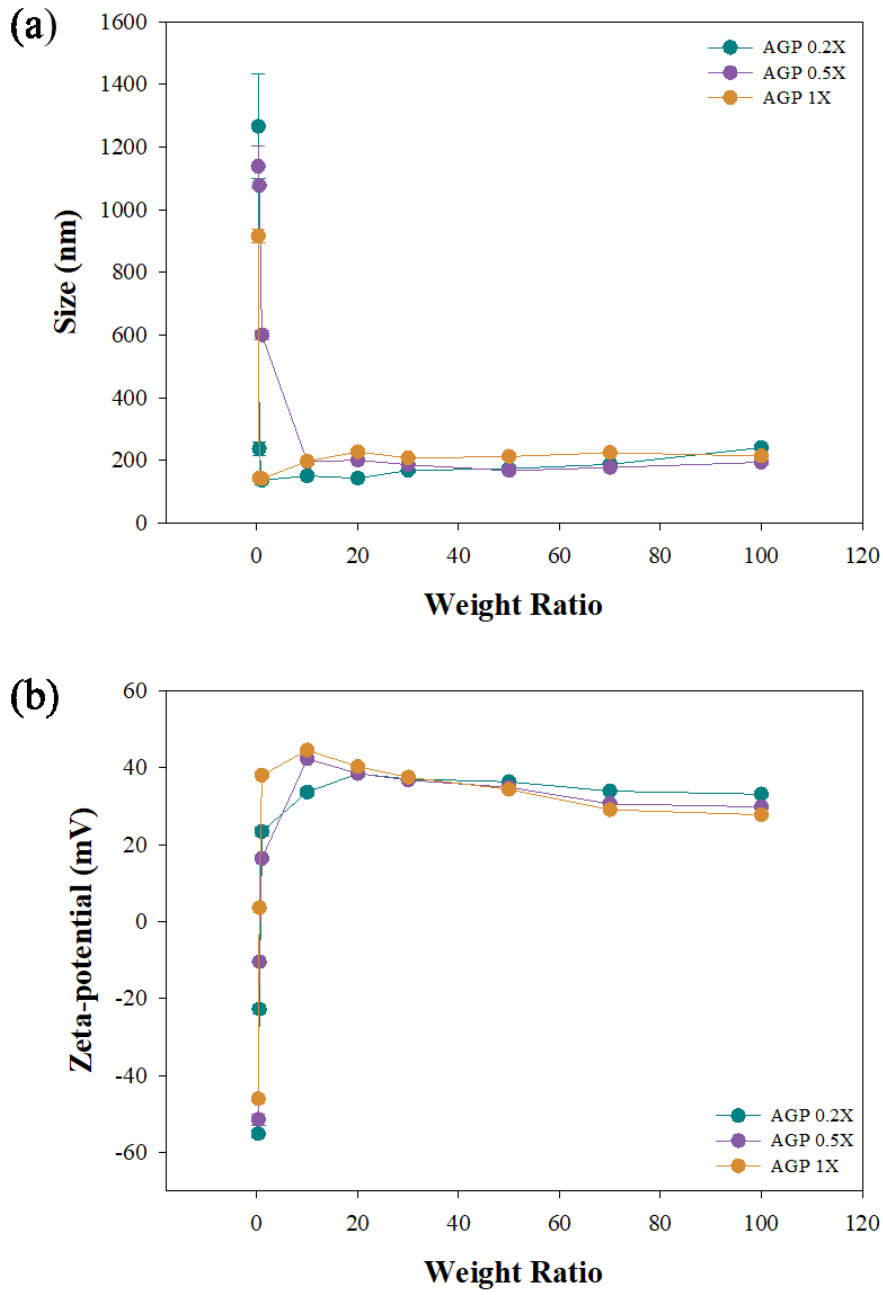

Figure 10. (a) Z-average size and (b) zeta-potential of AGP/pDNA polyplexes at various weight ratios.

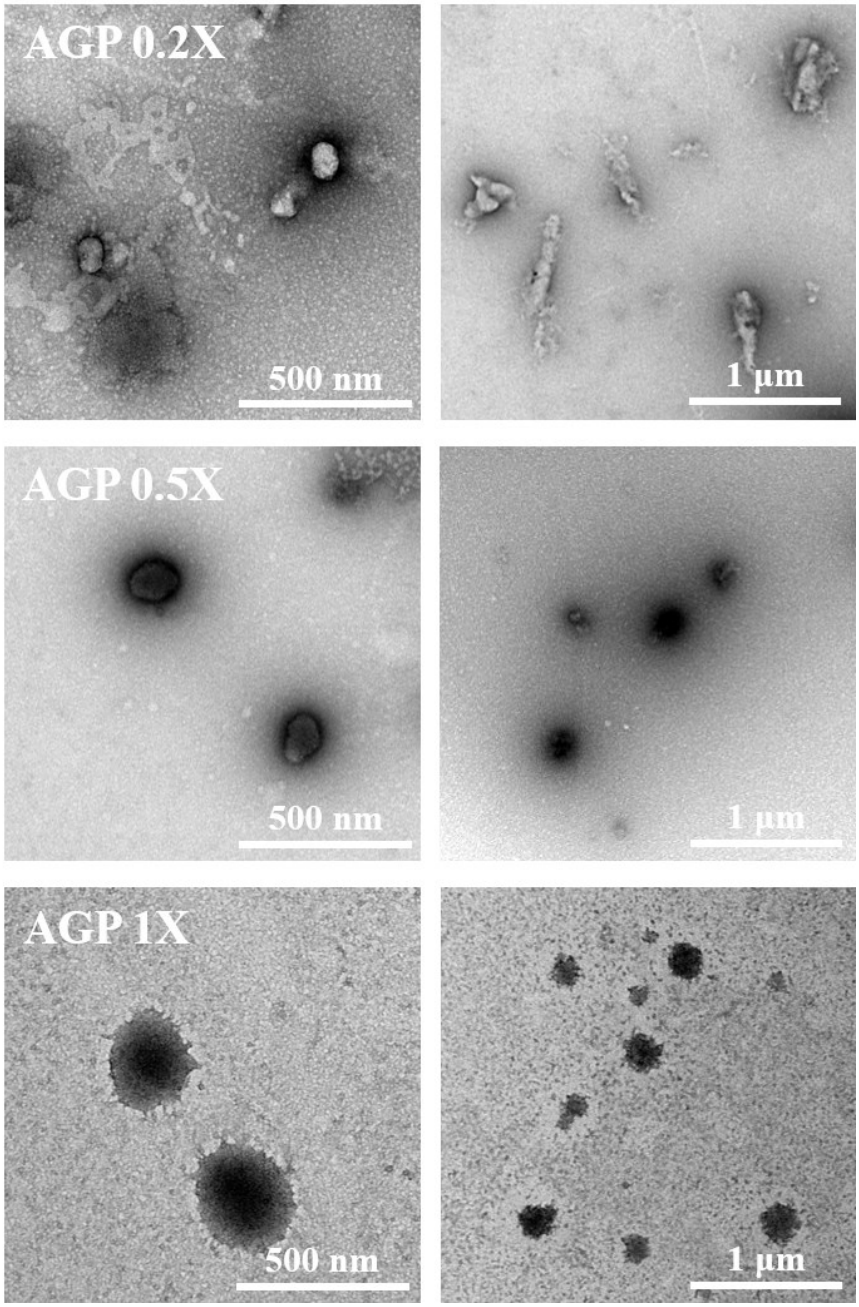

Figure 11. TEM images of AGP/pDNA polyplexes. All polyplexes were formed at a weight ratio of 10.

4.2.6. Heparin competition assay

Heparin, a negatively charged substance, can be utilized as a competitor of pDNA. By adding heparin at various concentrations to the polyplex solution, the stability of the polyplex can be analyzed [42]. In the research, a heparin competition assay was conducted for AGP0.5X (**Figure 12**). PEI25k/pDNA polyples released pDNA at low concentrations of heparin treated. Although AGP0.5X/pDNA polyplex at a weight ratio of 1 showed similar pDNA retardation ability to PEI25k/pDNA polyplex, retardation ability was improved as the weight ratio increased. At a weight ratio of 10, the pDNA band was detected at a high heparin concentration (8 mg/mL), indicating stable polyplex formation of AGP 0.5X. This result demonstrates that AGP0.5X forms a very compact and stable polyplex compared to other functionalized polysaccharides previously reported. Sucrose-crosslinked PEI polyplex released pDNA at 1.0-1.1 mg/mL of heparin concentration [43] and zoledronic acid-loaded cationic methylcellulose polyplex released pDNA at 2.0 mg/mL [44]. The strong binding ability of AGP 0.5X to pDNA is speculated to be due to the high flexibility of the polymer and hydrogen bonding between the AGP 0.5X and pDNA [45].

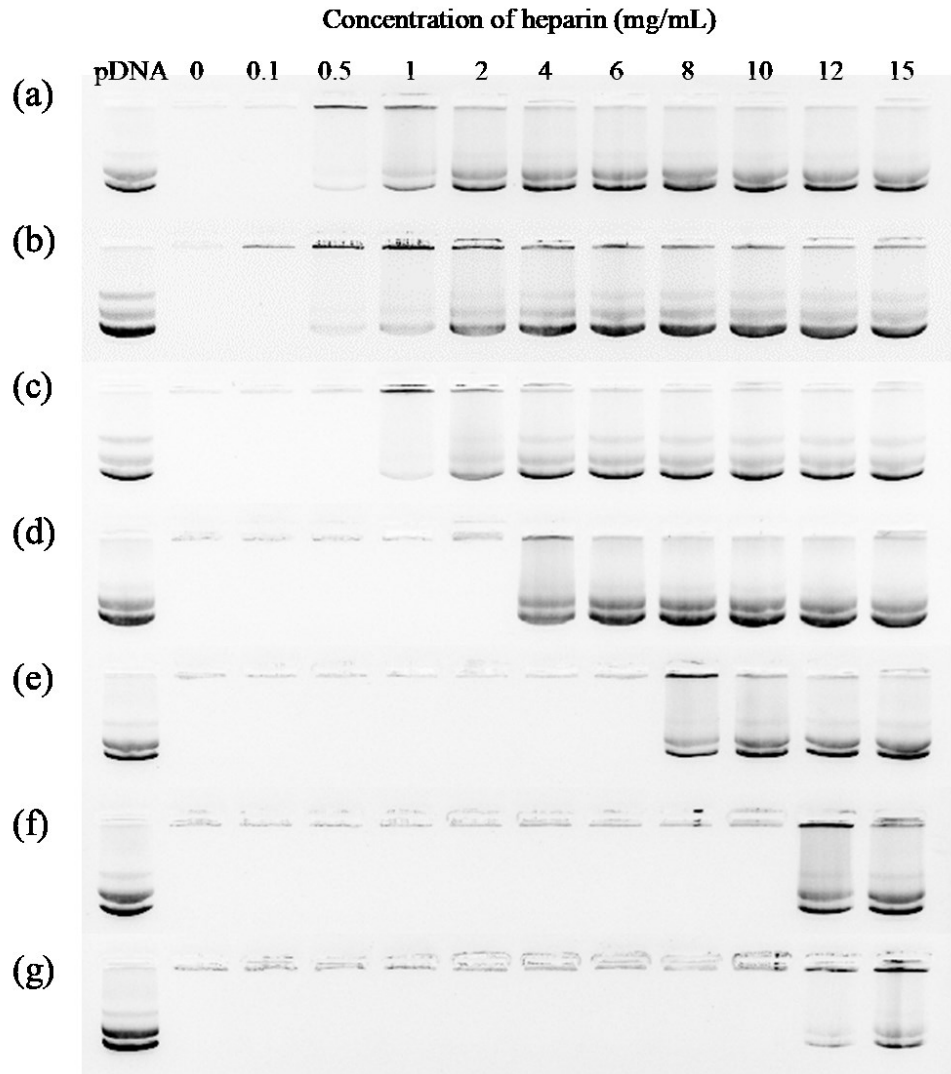

Figure 12. Heparin competition assay results of (a) PEI25k/pDNA polyplexes at wr 1 (b) and AGP 0.5X/pDNA polyplexes at wr 1 (c), wr 2 (d), wr 5 (e), wr 10 (f), wr 20, and (g) wr 30.

4.2.7. pDNA protection from serum protein

When polyplexes are injected into the body, genes can be degraded by various serum proteins including nucleases [46]. In order to achieve effective gene delivery, genes must be protected from serum proteins by their carrier [47]. To assess pDNA protection of AGP 0.5X, polyplexes were formed at high concentrations of FBS and heparin, and the degradation of pDNA was examined.

As shown in **Figure 13**, pDNA (lane 2) was degraded when it was incubated with FBS and heparin, showing smeared a band. The same result was observed with PEI25k/pDNA and AGP 0.5X/pDNA polyplexes at low weight ratios (1, 2, 5). However, at a weight ratio of 10 and higher, AGP 0.5X successfully protected pDNA from degradation.

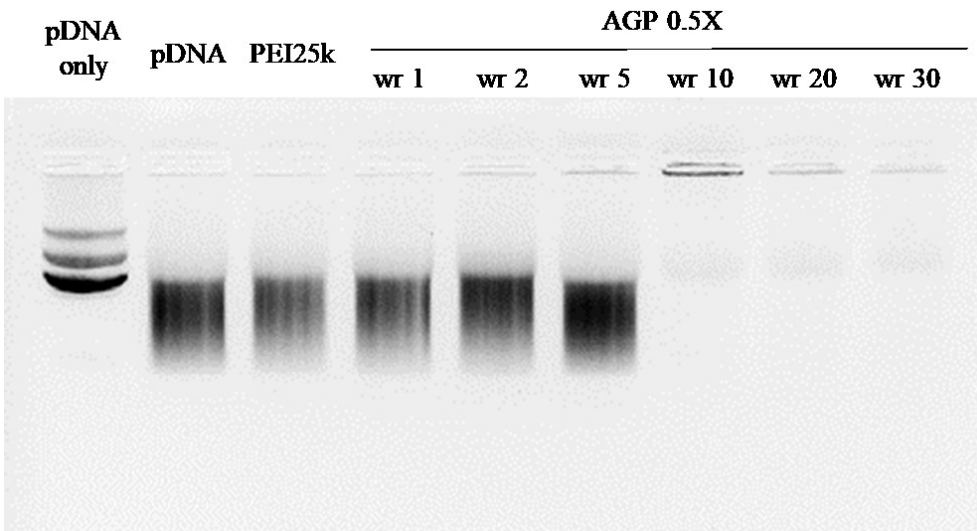

Figure 13. pDNA protection ability of AGP/pDNA polyplexes from serum nuclease. Except for lane 1 (pDNA only), all polyplexes were incubated in the presence of FBS (50%) and heparin (4 mg/mL).

4.3. *In vitro* assay of AGP and AGP/pDNA polyplex

4.3.1. Cytotoxicity of AGP

Cytotoxicity of AGPs was evaluated by measuring cell metabolic activity via MTT assay in HepG2, Hep3B, and HeLa cells (**Figure 14**). In the case of PEI25k, relative cell viability (RCV) decreased dependently on polymer concentration for all three cells, confirming that PEI25k possesses high cytotoxicity. Meanwhile, AGP 0.2X, 0.5X, and 1X showed higher RCV than PEI25k for all cells. Especially, high RCV was observed consistently even at the increased concentration of AGP for HepG2 and Hep3B. Although AGP 0.2X exhibited the lowest toxicity when it was treated with 70 μg/mL, overall, there was no significant difference in cytotoxicity among AGP 0.2X, 0.5X, and 1X. In HeLa cells, RCV was below 70% when the polymer concentration was over 30 and gradually decreased as the treatment concentration increased. HeLa cells are known to have a higher sensitivity to toxicity compared to hepatocytes. Considering the cytotoxicity of AGPs in HeLa cells, further experiments were performed at low weight ratios (up to 30).

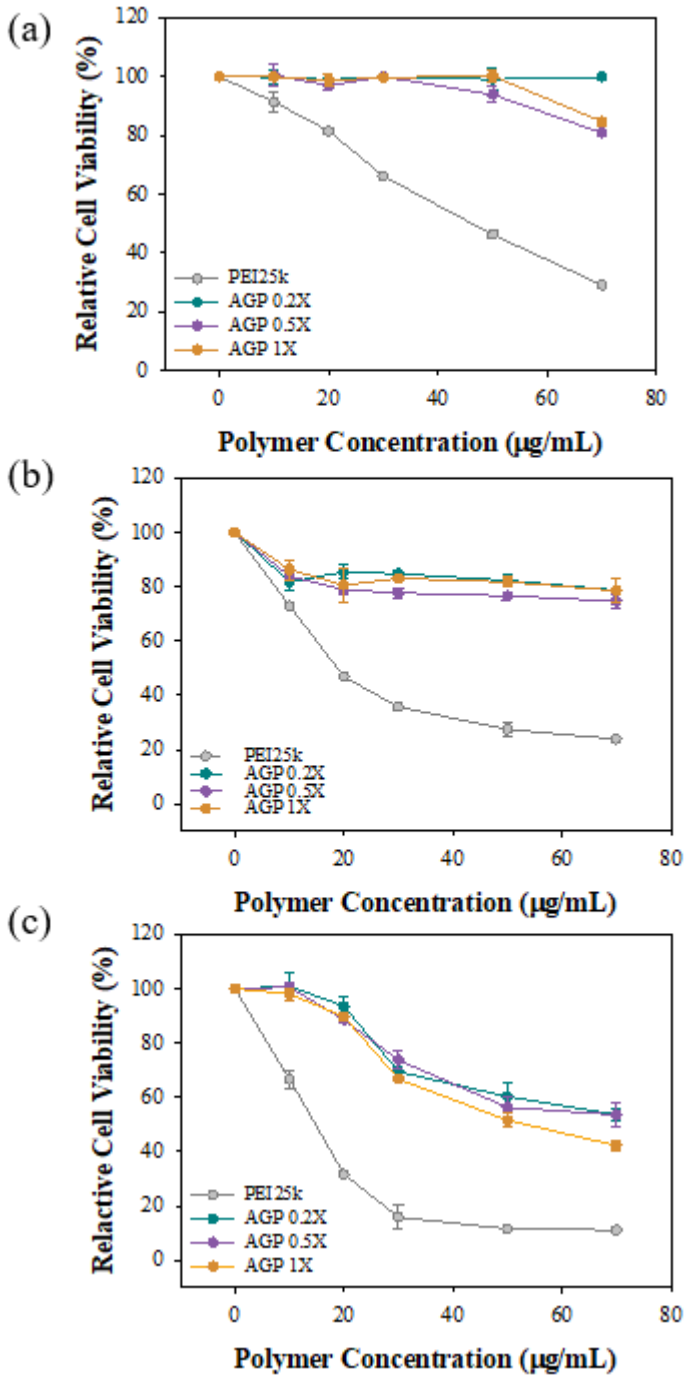

Figure 14. MTT assay results of (a) HepG2, (b) Hep3B, and (c) HeLa cells. PEI25k was used as a positive control.

4.3.2. Luciferase transgene expression assay

Luciferase transgene expression assay was performed to examine the transfection efficiency of AGPs. pCN-Luci (pDNA), which expresses luciferase protein, was utilized as the reporter gene. Transfection efficiency was calculated based on the luminescence generated from the reaction between luciferin and the expressed luciferase, and the amount of protein in the sample.

Firstly, the transfection efficiency of AGP 0.2X, 0.5X, and 1X was measured in serum-free conditions in HepG2, Hep3B, and HeLa cells (**Figure 15**). Compared to AGP 0.2X and AGP 1X, AGP 0.5X exhibited the highest transfection efficiency in HepG2 cells. In particular, the transfection efficiency exceeded PEI25k at weight ratios of 10 and 20. As a result, AGP 0.5X was selected as the optimal gene carrier, and further experiments were conducted with AGP 0.5X (subsequently named AGP).

To determine the optimal weight ratio of AGP/pDNA polyplexes, luciferase transgene assay was performed at various weight ratios (1, 2, 5, 10, 20, 30) in both serum-free and serum-containing conditions (**Figure 16**). In the case of HepG2 and Hep3B, transfection efficiency increased until reaching a weight ratio of 5 or 10 and gradually decreased. Considering the superior physiochemical properties of a weight ratio of 10 compared to 5, AGP 0.5X at a weight ratio of 10 was optimized as the final gene delivery system. Further experiments were conducted at a weight ratio of 10.

Meanwhile, the ASGPR targeting ability of AGP 0.5X was assessed by treating free galactose (1 mM). Pre-treated galactose binds to ASGPR and induces turn-over of the receptor, inhibiting further receptor-mediated endocytosis. As shown in Figure 17, treatment of free galactose significantly decreased transfection efficiency in HepG2 cells. While the transfection efficiency of galactose pre-treated PEI25k/pDNA polyplexes decreased to 59.87%, AGP/pDNA polyplexes at a weight ratio of 10 decreased to 3.30%. In the case of Hep3B cells, a notable decrease was observed, but the level was not as high as that of HepG2. This is because the expression levels of ASGPR vary depending on the cell line. HeLa cells showed negligible change in transfection efficiency. This proves the ability of AGP to target ASGPR, suggesting its potential as an excellent gene delivery system for HCC-targeted therapy.

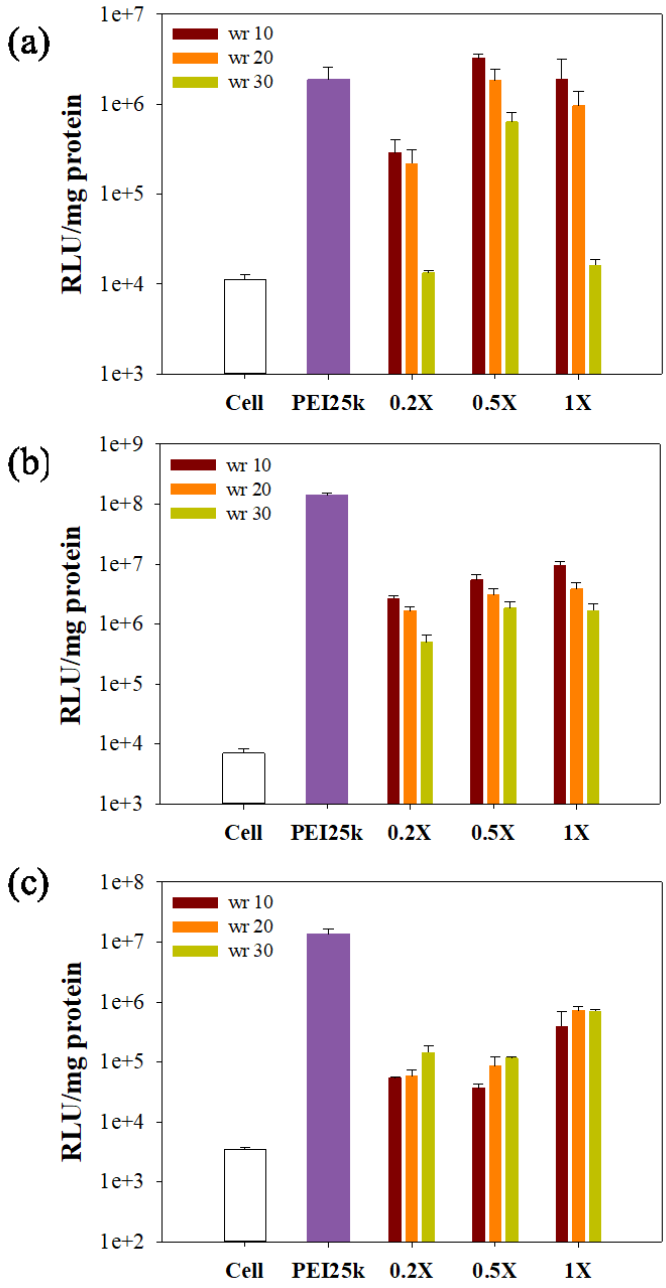

Figure 15. Luciferase transgene expression assay results of AGP/pDNA polyplexes in (a) HepG2, (b) Hep3B, and (c) HeLa cells. 0.2X, 0.5X, and 1X refer to AGP 0.2X, AGP 0.5X, and AGP 1X, respectively. PEI25k/pDNA (wr 1) was used as a positive control.

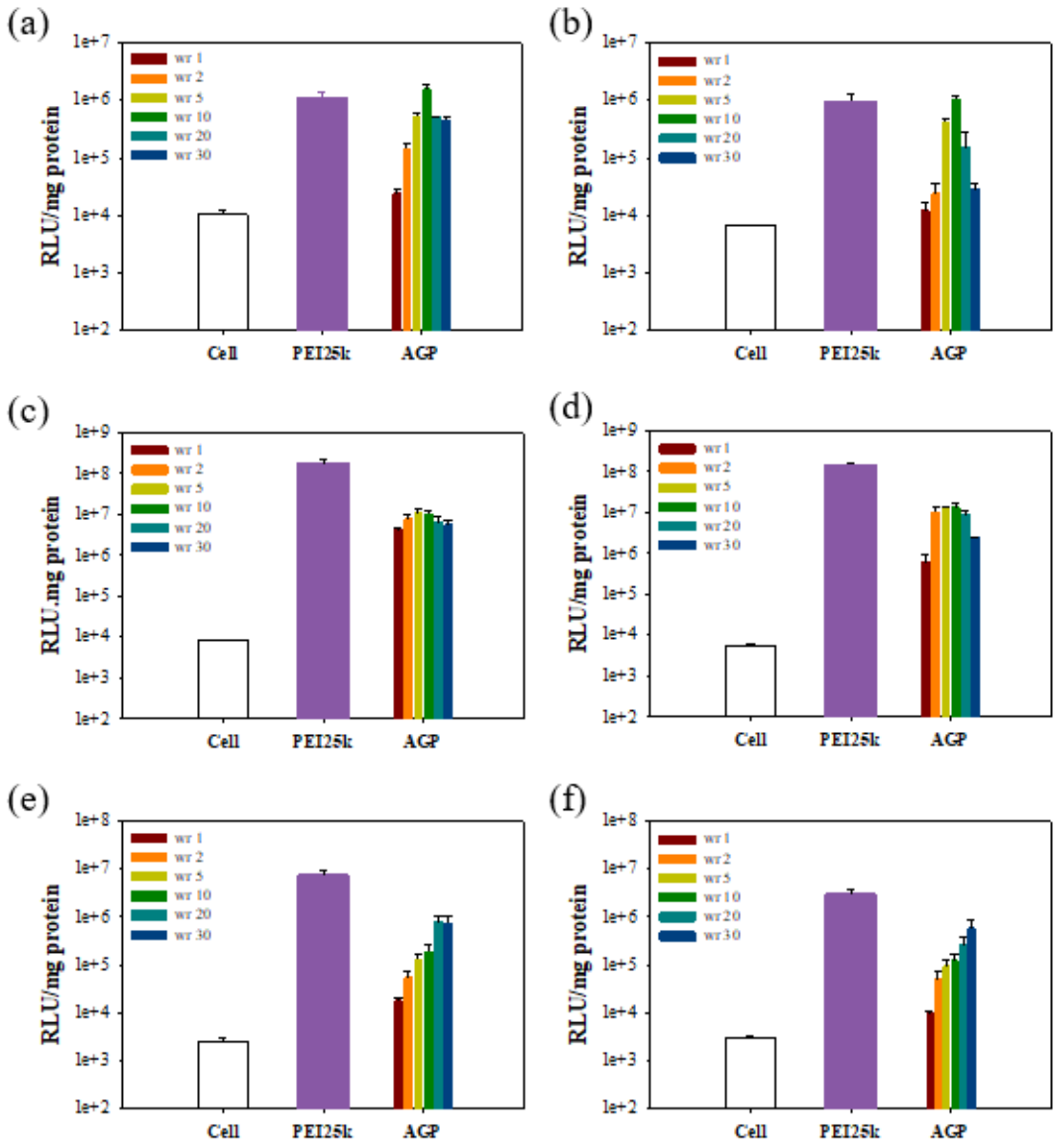

Figure 16. Luciferase transgene expression assay results of AGP/pDNA polyplexes at various weight ratios (a–b) HepG2 (c–d), Hep3B, and (e–f) HeLa cells. (a, c, e) Serum–free condition and (b, d, f) serum condition. PEI25k/pDNA (wr 1) was used as a positive control.

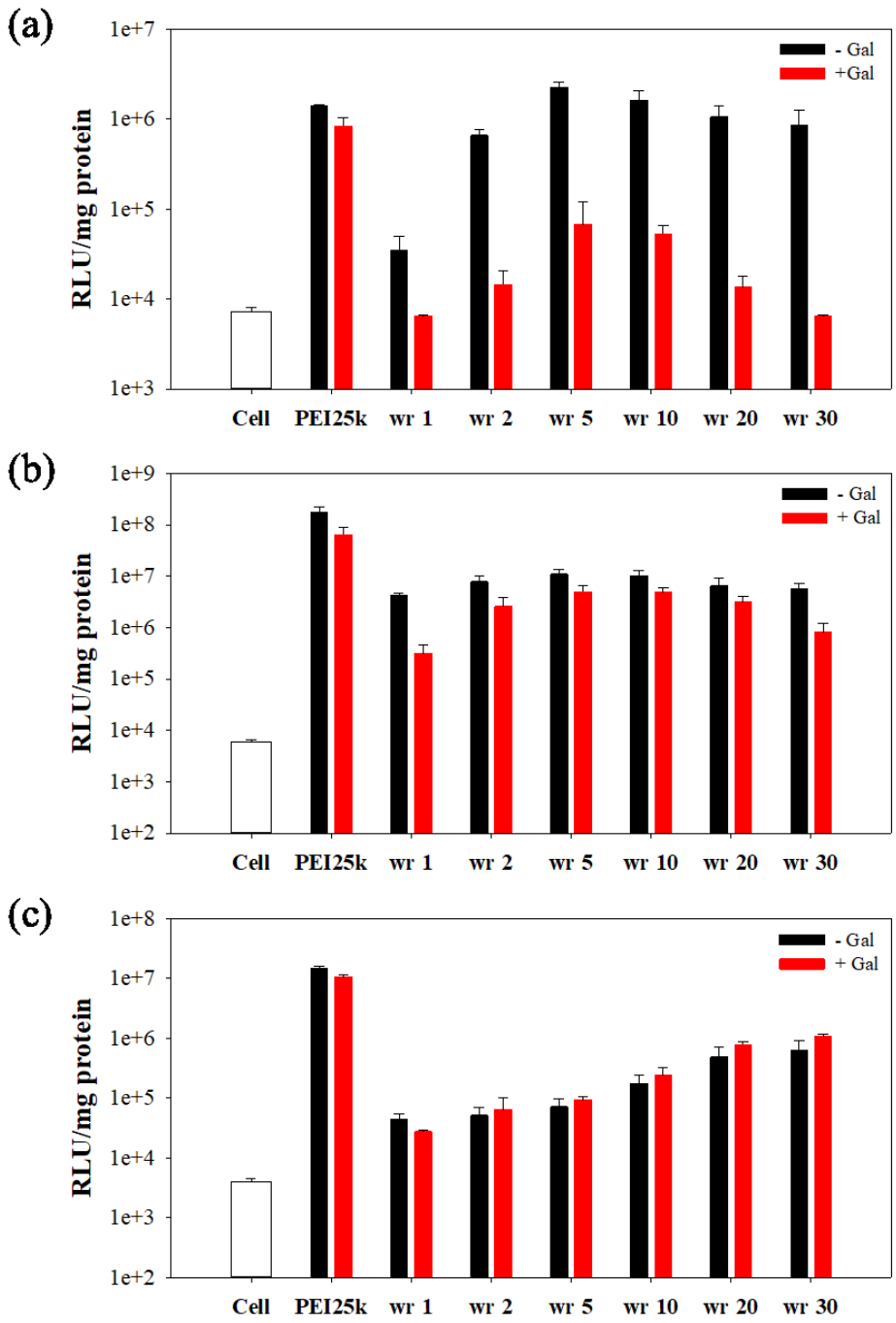

Figure 17. Luciferase transgene expression assay results of AGP/pDNA polyplexes with or without galactose (1 mM) competition in (a) HepG2, (b) Hep3B, and (c) HeLa cells. PEI25k/pDNA (wr 1) was used as a positive control.

4.3.3. Cellular uptake

Cellular uptake of AGP/pDNA polyplexes was analyzed by detecting the fluorescence of YOYO-1 iodide labeled pDNA. The relative cellular uptake for PEI25k/pDNA and AGP/pDNA polyplexes in HepG2 cells was 40.6% and 30.2%, respectively. Despite the active targeting ability of AGP, the higher cellular uptake efficiency of PEI25k may be due to the gravity that occurs *in vitro* experiments. In 2D cell culture, polyplexes can settle by gravity and can be taken up by cells attached to the culture plate due to the absence of the external flow which exists in the actual human body. In addition, high cellular uptake does not always result in high transfection efficiency because the polyplexes undergo various intracellular steps after entering the cells such as endosomal escape. Meanwhile, the relative cellular uptake for PEI25k/pDNA and AGP/pDNA polyplexes in HeLa cells was 93.9% and 83.5%, respectively.

To further confirm the ASGPR-targeting ability of AGP in hepatocytes, a galactose competition assay was conducted. The relative cellular uptake of AGP/pDNA polyplexes dramatically decreased to 37.09% in HepG2 while insignificant change was recognized in Hep3B (99.13%) and HeLa cells (99.28%). The cellular uptake of PEI25k/pDNA polyplexes was consistent in all cell lines, regardless of galactose treatment. This result supports the ASGPR-targeting ability of AGP.

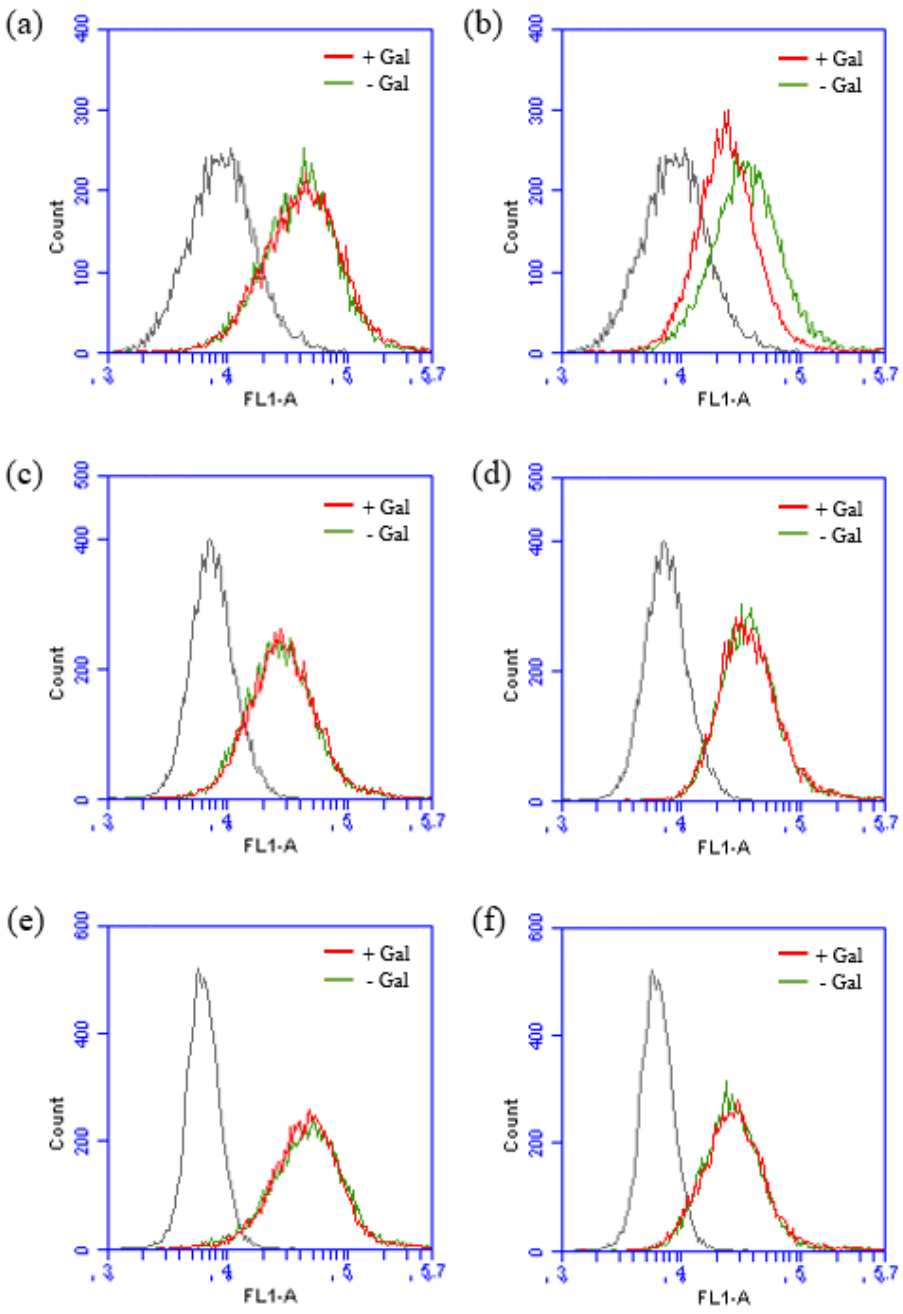

Figure 18. Cellular uptake of PEI25k/pDNA and AGP/pDNA polyplexes with or without galactose (1 mM) competition in (a–b) HepG2, (c–d) Hep3B, and (e–f) HeLa. (a, c, e) PEI25k/pDNA polyplexes and (b, d, f) AGP/pDNA polyplexes.

4.3.4. Intracellular trafficking visualization

To examine the intracellular trafficking of AGP/pDNA polyplexes in hepatocytes, polyplexes were treated to HepG2 for 2 h, 4 h, and 8 h and observed by CLSM (**Figure 19-21**). pDNA was labeled with YOYO-1 iodide (green), acidic organelles were labeled with Lysotracker red DND-99 (red), and nuclei were labeled with DAPI (blue). The colocalization of pDNA with nuclei and lysosome were examined by calculating Pearson's coefficient (**Figure 22**).

After 2 h of treatment, the majority of the green fluorescence of PEI/pDNA and AGP/pDNA polyplexes were detected in the cytoplasm, and some were observed in the nucleus. It was noticeable that AGP/pDNA polyplexes approached to more population of cells than PEI/pDNA polyplexes. This may suggest that AGP has a higher affinity for hepatocytes compared to PEI. After 4 h of treatment, colocalization between the nucleus and pDNA increased in both PEI/pDNA and AGP/pDNA. After 8 h of treatment, only a few green signals were detected, indicating that most of the pDNA escaped the lysosome and reached the nuclei. AGP/pDNA delivered pDNA to nearly all HepG2 cells while PEI/pDNA polyplex delivered pDNA to a small portion of the total cell population. This may be due to the ability of AGP in forming stable nanoparticles and safely protecting pDNA mentioned above. In addition, the affinity of AGP to ASGPR may have resulted in the superior intracellular trafficking behavior of AGP in hepatocytes.

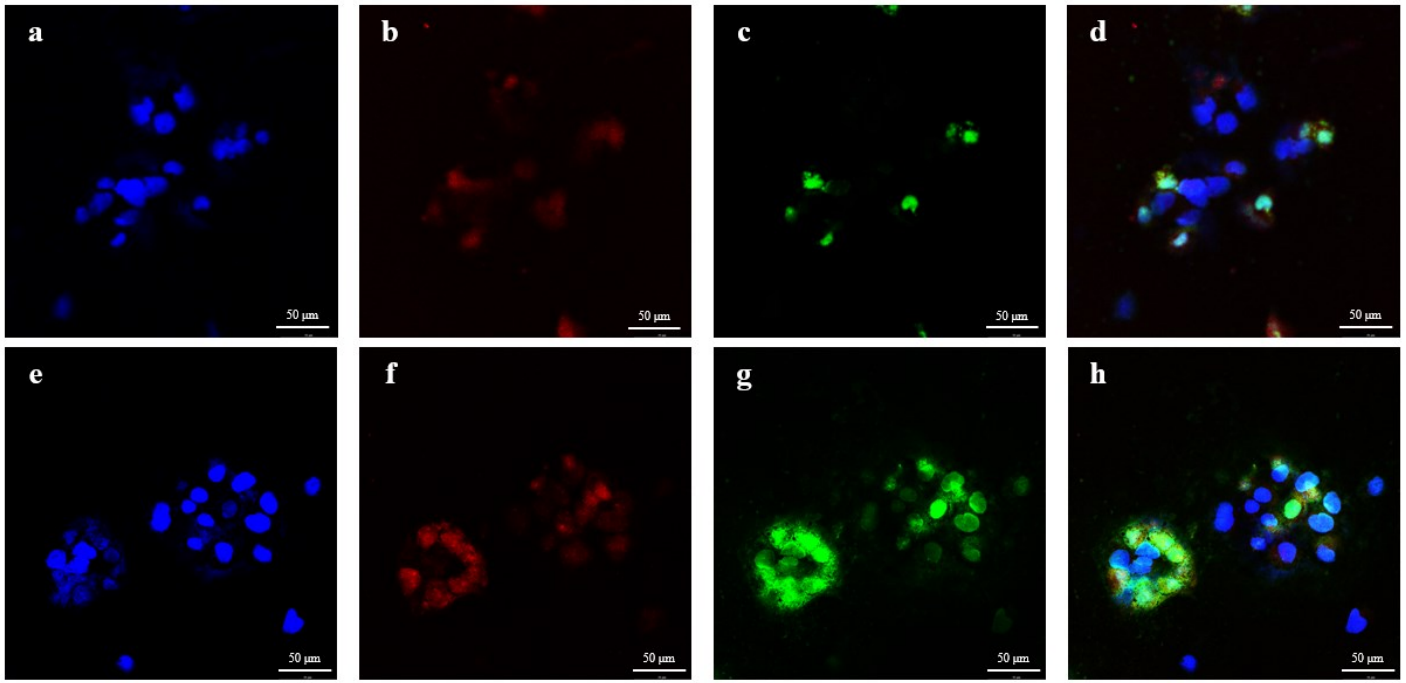

Figure 19. CLSM images of PEI25k/pDNA (wr 1) (a-d) and AGP/pDNA (e-h) after 2 h of treatment in HepG2 cells. DAPI (blue) stained nuclei (a, e), Lysotracker red DND-99 (red) stained acidic organelles (b, f), YOYO-1 (green) stained pDNA (c, g), and merged image (d, h).

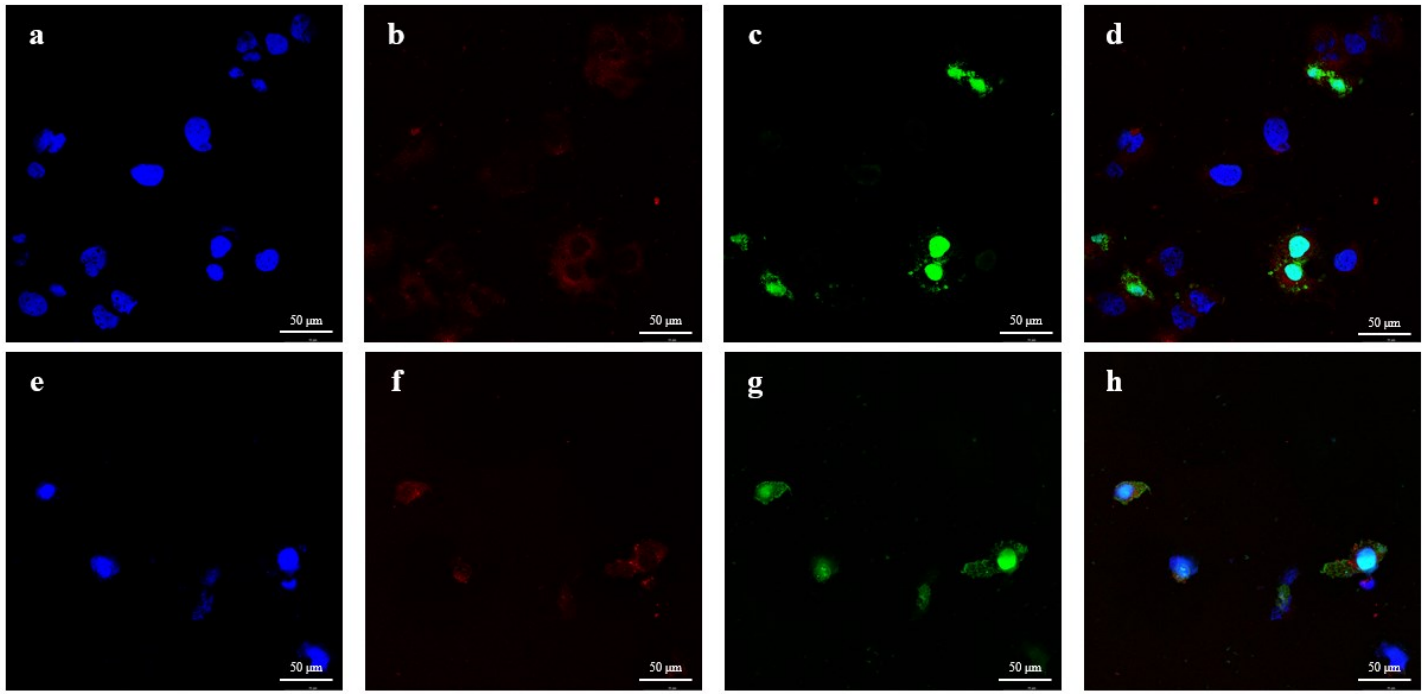

Figure 20. CLSM images of PEI25k/pDNA (wr 1) (a-d) and AGP/pDNA (e-h) after 4 h of treatment in HepG2 cells. DAPI (blue) stained nuclei (a, e), Lysotracker red DND-99 (red) stained acidic organelles (b, f), YOYO-1 (green) stained pDNA (c, g), and merged image (d, h).

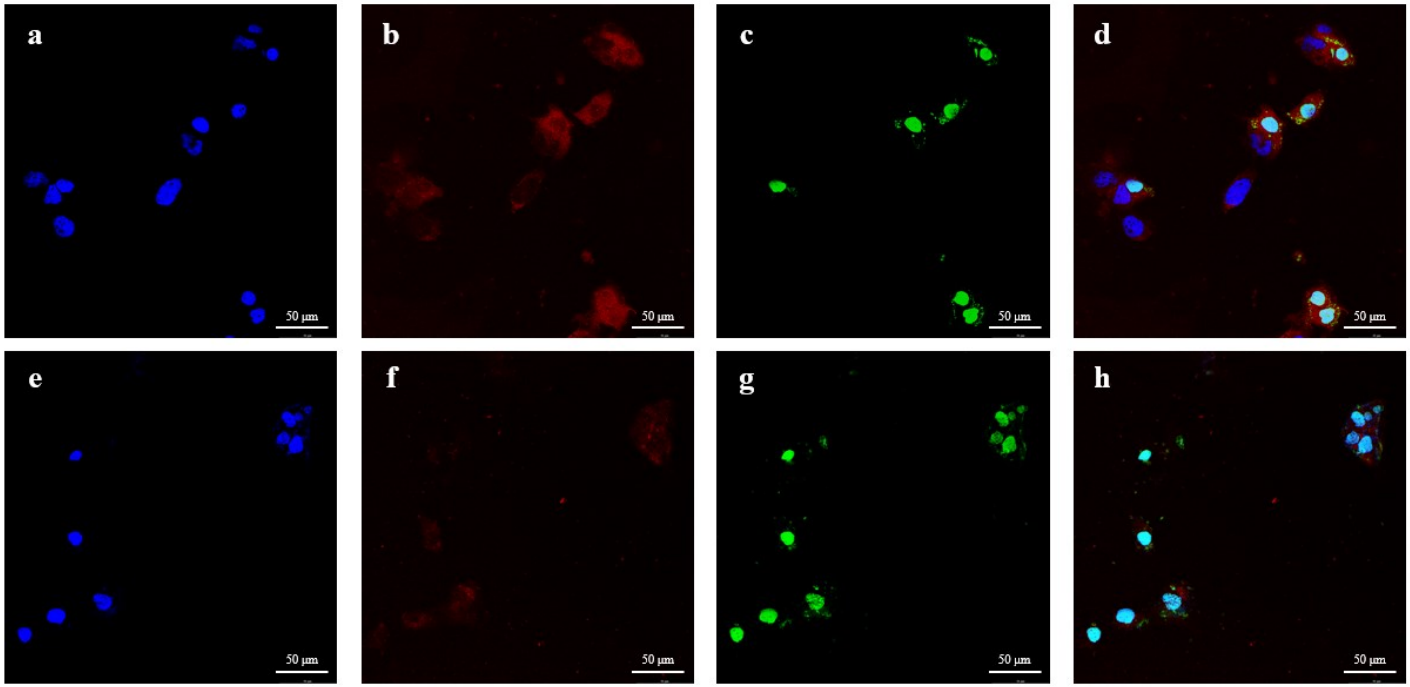

Figure 21. CLSM images of PEI25k/pDNA (wr 1) (a-d) and AGP/pDNA (e-h) after 4 h of treatment and 4 h of post-incubation in HepG2 cells. DAPI (blue) stained nuclei (a, e), Lysotracker red DND-99 (red) stained acidic organelles (b, f), YOYO-1 (green) stained pDNA (c, g), and merged image (d, h).

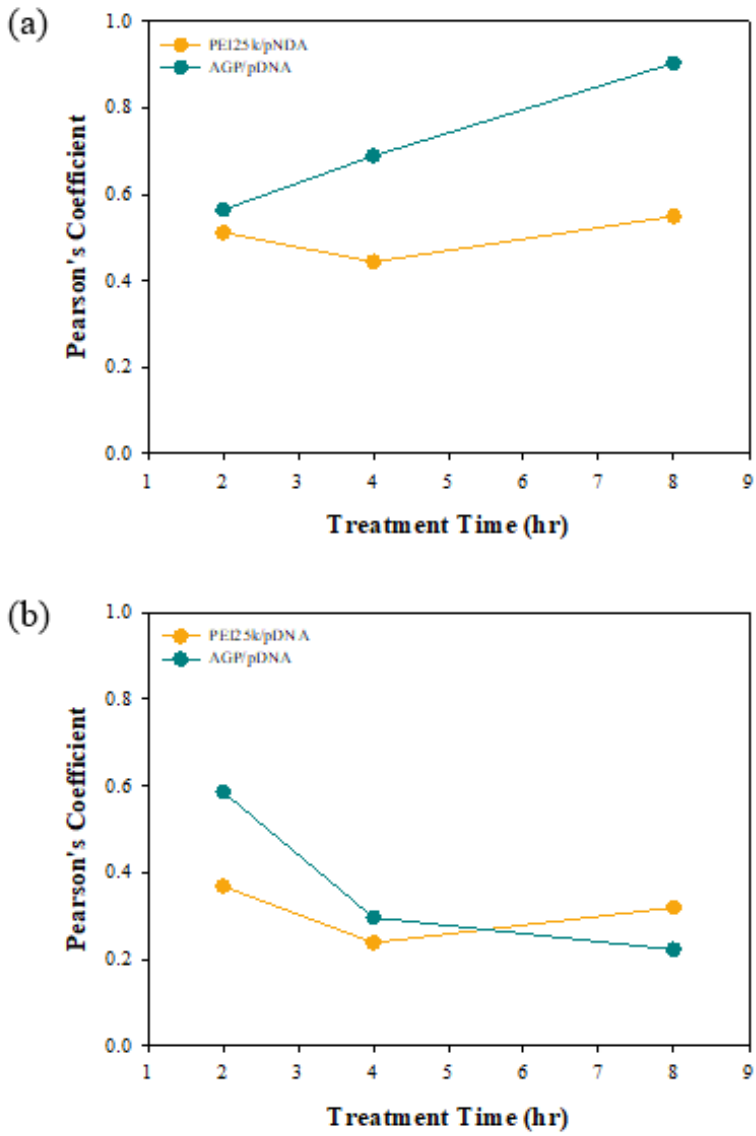

Figure 22. Pearson's coefficient used to analyze the colocalization of YOYO-1 and DAPI (a), and YOYO-1 and lysotracker red (b). The coefficient was calculated based on the fluorescence signals in one representative image for each sample which were shown in Figure 19-22. Pearson's coefficient range from -1 which implies anti-correlation to +1 which stands for the perfect correlation.

4.4. Antitumor effect of AGP/siRNA

4.4.1. Characterization of AGP/siRNA

The experiments were optimized with AGP 0.5X at a weight ratio of 10 as the HCC-targeted gene delivery system. Bcl-2 siRNA was complexed with AGP to form AGP/siRNA. The measured average size and zeta-potential value of AGP/siRNA were 156.06±6.22 nm and 48.25±0.55 mV, respectively.

4.4.2. Bcl-2 silencing effect

Bcl-2 mRNA expression level was analyzed by RT-qPCR (**Figure 23**). Successful siRNA delivery results in the reduction of Bcl-2 mRNA due to the cleavage by the RISC/siRNA complex. Free siRNA treated sample showed a negligible decrease in relative Bcl-2 mRNA expression level (95.02%). In the case of PEI/siRNA and AGP/siRNA, expression levels significantly decreased to 35.56% and 27.90%, respectively. This result correlates with superior intracellular trafficking and transfection efficiency of AGP compared to PEI proven above.

4.4.3. Antitumor effect analysis with MTT assay

The antitumor effect of AGP/siRNA was examined by MTT assay in HepG2 cells (**Figure 24**). Relative cell viability (RCV) of free siRNA, PEI/siRNA, and AGP/siRNA treated cells were 94.62%, 91.90%, and 71.58%, respectively. Although AGP/siRNA showed a

noticeable decrease in RCV compared to control and other samples, it was not as significant as the downregulated expression of Bcl-2 mRNA demonstrated previously. Similarly, while Bcl-2 expression significantly decreased in PEI/siRNA treated cells, the degree of cell death was not as pronounced. The process of cell apoptosis is complex and requires various processes beyond inhibiting Bcl-2 protein production to trigger apoptosis [48]. Cell death is followed by the complete breakdown of the plasma membrane and the acquisition of a necrotic morphotype [49]. Therefore, additional strategies such as co-delivery of anticancer drugs and siRNA may be necessary to achieve a more enhanced antitumor effect.

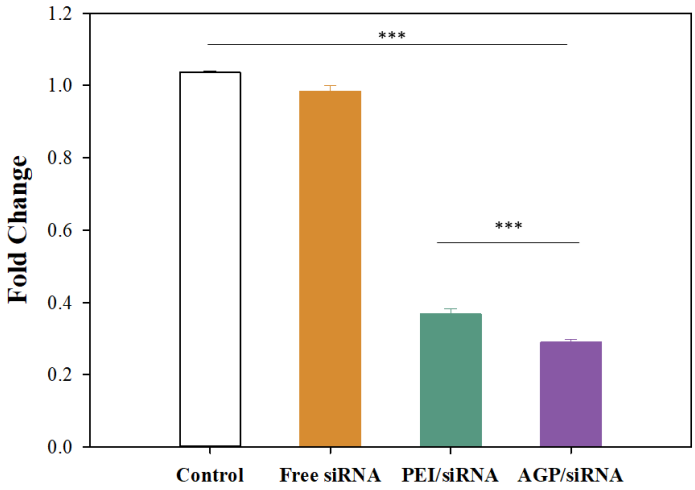

Figure 23. Real-time qPCR results of Bcl-2 mRNA expression levels from HepG2 after treatment of free Bcl-2 siRNA, PEI/siRNA, and AGP/siRNA. Statistical analysis was proceeded through one-way ANOVA and Bonferroni post-hoc test. ($P < 0.05$ *, $P < 0.01$ **, $P < 0.001$ ***)

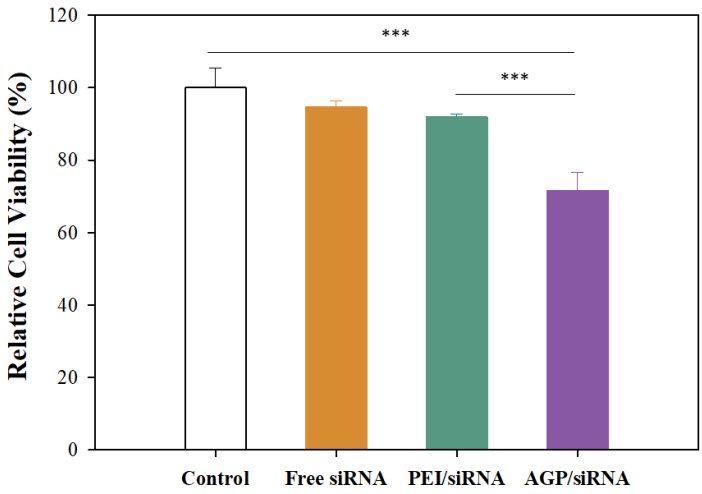

Figure 24. Relative cell viability of HepG2 after treatment of free Bcl-2 siRNA, PEI/siRNA, and AGP/siRNA. Statistical analysis was proceeded through one-way ANOVA and Bonferroni post-hoc test. ($P < 0.05$ *, $P < 0.01$ **, $P < 0.001$ ***)

4.4.4. Apoptosis induction test with Annexin V staining

Annexin V staining was performed to authenticate that AGP/siRNA induces cell death through apoptosis. Alexa fluor 488 (FL1) was used to stain pro-apoptotic cells and propidium iodide (FL2) was used to label dead cells. The color compensation was proceeded (FL2-5.80% FL1, FL1-5.00% FL2) to correct the error produced by the overlap of two fluorescence dyes. As shown in **Figure 25**, the untreated cells and AGP/siRNA treated cells showed 15.3% and 45.2% of cell death by apoptosis, respectively. This result indicates that AGP successfully delivered Bcl-2 siRNA and induced apoptosis.

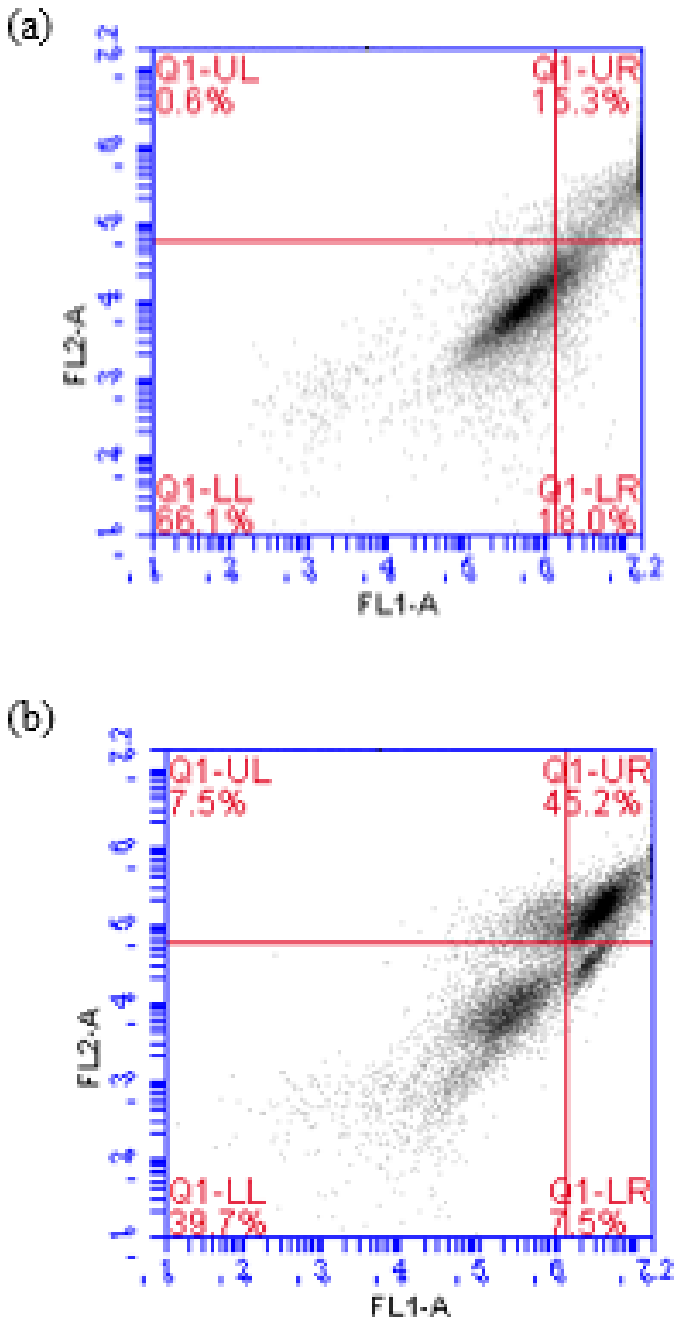

Figure 25. Flow cytometry results of annexin V staining of (a) untreated cells and (b) AGP/siRNA treated cells. (FL1: Alexa Flour 488, FL2: PI).

Chapter 5. Conclusion

In this study, polyethyleneimine-conjugated arabinogalactan (AGP) was synthesized and evaluated as a hepatocellular carcinoma-targeted gene delivery system. Arabinogalactan (AG) from *Larch* tree, which is mainly composed of galactose and arabinose, was hypothesized to have the ability to target asialoglycoprotein receptor (ASGPR) overexpressed in hepatocytes.

Using the newly developed one-pot synthesis method, PEI (Mw 10,000 Da) was conjugated to AG with different degrees of oxidation. Successful conjugation was confirmed by ^{1}H NMR, FT-IR, and GPC measurements. AGPs could form positively charged nanoparticles. AGP 0.5X especially formed a stable sphere-shaped polyplex with a smooth surface and exhibited pDNA protecting ability against serum proteins.

AGPs showed low cytotoxicity towards hepatocytes (HepG2, Hep3B). AGP 0.5X/pDNA polyplexes at a weight ratio of 10 exhibited the highest transfection efficiency in HepG2 cells. Meanwhile, transfection efficiency and cellular uptake of AGP 0.5X/pDNA polyplexes decreased significantly in ASGPR overexpressed cells when pre-treated with free galactose. Also, AGP0.5X/pDNA polyplexes showed superior affinity to HepG2 compared to PEI, proving its ASGPR targeting ability. AGP/siRNA, AGP 0.5X complexed with Bcl-2 siRNA, successfully inhibited Bcl-2 mRNA expression and led to an antitumor effect. It was confirmed that the

cell death induced by AGP/siRNA occurred via apoptosis. Consequently, it is concluded that AGP possesses great potential as a promising HCC-targeted gene delivery carrier.

References

[1] J. M. Llovet, J. Zucman-Rossi, E. Pikarsky et al., Hepatocellular carcinoma, Nature Reviews Disease Primers, 2016, 2, 16018.

[2] J. M. Llovet, R. Pinyol, R.K. Kelly et al., Molecular pathogenesis and systemic therapies for hepatocellular carcinoma, Nature Cancer, 2022, 3, 386-401.

[3] H. Zhang, W. Zhang, L. Jiang et al., Recent advances in systemic therapy for hepatocellular carcinoma, Biomarker Research, 2022, 10 (3).

[4] M. Maluccio and A. Covey, Recent progress in understanding, diagnosing, and treating hepatocellular carcinoma, CA: A Cancer Journal for Clinicians, 2012, 62(6), 394-399.

[5] S. C. Reghupaty, and D. Sarkar, Current Status of Gene Therapy in Hepatocellular Carcinoma, Cancers (Basel), 2019, 11(9), 1265.

[6] A. Yusuf, A. R. Z. Almotairy, H. Henidi, O. Y. Alshehri, and M. S. Aldughaim, Nanoparticles as Drug Delivery Systems: A Review of the Implication of Nanoparticles' Physicochemical Properties on Responses in Biological Systems, Polymers, 2023, 15(7), 1596.

[7] D. Roggenbuck, M. G. Mytilinaiou, S. V. Lapin et al., Asialoglycoprotein receptor (ASGPR): a peculiar target of liver-specific autoimmunity, Autoimmun Highlights, 2012, 3, 119-125.

[8] H. Wang, S. Shi, B. Bao et al., Structure characterization of an arabinogalactan from green tea and its anti-diabetic effect, Carbohydrate Polymers, 2015, 124, 98-108.

[9] A. D. Mola, F. F. Summa et al., Synergistic Properties of Arabinogalactan (AG) and Hyaluronic Acid (HA) Sodium Salt Mixtures, Molecules, 2021, 26(23), 7246.

[10] E. M. Goellner, J. Utermoehlen, R. Kramer, and B. Classen, Structure of arabinogalactan from Larix laricina and its reactivity with antibodies directed against type-II-arabinogalactans, Carbohydrate Polymers, 2011, 86(4), 1739-1744.

[11] A. A. D' Souza, and P. V. Deverajan, Asialoglycoprotein receptor mediated hepatocyte targeting - Strategies and applications, Journal of Controlled Release, 2015, 203, 126-139.

[12] G. Ahn, S. Banik, C. Bertozzi et al., LYTACs that engage the asialoglycoprotein receptor for targeted protein degradation, Nature Chemical Biology, 2021, 17(9), 937-946.

[13] Z. Ye, W. Wu, Y. Qin et al., An Integrated Therapeutic Delivery System for Enhanced Treatment of Hepatocellular Carcinoma, Advanced Functional Materials, 2018, 28(18), 1706600.

[14] S. Xu, S. Ling, Q. Shan et al., Self-Activated Cascade-Responsive Sorafenib and USP22 shRNA Co-Delivery System for Synergetic Hepatocellular Carcinoma Therapy, Advanced Science, 2021, 8(5), 2003042.

[15] R. I. Pinhassi, Y. G. Assaraf, S. Farber, Y. D. Livney et al., Arabinogalactan–Folic Acid–Drug Conjugate for Targeted Delivery and Target–Activated Release of Anticancer Drugs to Folate Receptor–Overexpressing Cells, Biomacromolecules, 2010, 11(1), 294–303

[16] P. O. Pathak, M. S. Nagarsenker, A. Fahr et al., Cholesterol anchored arabinogalactan for asialoglycoprotein receptor targeting: synthesis, characterization, and proof of concept of hepatospecific delivery, Carbohydrate Research, 2015, 408, 33–43

[17] D. Hanahan, R. A. Weinberg, The hallmarks of cancer, Cell, 2000, 100(1), 57–70.

[18] S. Cory, D. Huang, and J. M. Adams, The Bcl–2 family: roles in cell survival and oncogenesis. Oncogene, 2003, 22, 8590–8607.

[19] R. J. Youle, and A. Strasser, The BCL-2 protein family: opposing activities that mediate cell death, Nature Reviews Molecular Cell Biology, 2008, 9(1), 47-59.

[20] J. Park, S. Kim, and T. Kim, Polyethylenimine-Conjugated Hydroxyethyl Cellulose for Doxorubicin/Bcl-2 siRNA Co-Delivery Systems, Pharmaceutics, 2023, 15(2), 708.

[21] R. L. Setten, J. J. Rossi, and S. Han, The current state and future directions of RNAi-based therapeutics, Nature Reviews Drug Discovery, 2019, 18, 421-446.

[22] D. Bumcrot, M. Manoharan, V. Koteliansky, and D. W. Y. Sah, RNAi therapeutics: a potential new class of pharmaceutical drugs, Nature Chemical Biology, 2006, 2, 711-719.

[23] H. Dana, G. M. Chalbatani, E. Gharagouzlo et al., Molecular Mechanisms and Biological Functions of siRNA, International Journal of Biomedical Science, 2017, 13(2), 48-57.

[24] R. V. Benjaminsen, M. A. Mattebjerg, T. L. Andersen et al., The possible "proton sponge " effect of polyethylenimine (PEI) does not include change in lysosomal pH, Molecular Therapy, 2013, 21(1), 149-157.

[25] G. Creusat, A. Rinaldi, G. Zuber et al., Proton Sponge Trick for pH-Sensitive Disassembly of Polyethylenimine-Based siRNA Delivery Systems, Bioconjugate Chemistry, 2010, 21(5), 994-1002.

[26] D. Jiang, and A. K. Salem, Optimized dextran-polyethylenimine conjugates are efficient non-viral vectors with reduced cytotoxicity when used in serum containing environments, International Journal of Pharmaceutics, 2012, 427(1), 71-79.

[27] Y. He, G. Cheng, L. Xie, Z. Gu et al., Polyethyleneimine/DNA polyplexes with reduction-sensitive hyaluronic acid derivatives shielding for targeted gene delivery, Biomaterials, 2013, 34(4), 1235-1245.

[28] Y. Tian, X. Liu, H. Liu, and J. Xing, Pathological changes of cochlear in deaf mice at different time after mouse cytomegalovirus infection, International Journal of Clinical and Experimental Medicine, 2015, 8(5), 7192-7197.

[29] H. Li, C. Dang, X. Tai, L. Xue, J. Zhang et al., VALD-3, a Schiff base ligand synthesized from o-vanillin derivatives, induces cell cycle arrest and apoptosis in breast cancer cells by inhibiting the Wnt/β-catenin pathway, Scientific Reports, 2021, 11, 14985.

[30] L. Diao, J. Tao, Y. Wang, Y. Hu, and W. He, Co-Delivery Of Dihydroartemisinin And HMGB1 siRNA By TAT-Modified Cationic Liposomes Through The TLR4 Signaling Pathway For Treatment Of Lupus Nephritis, International Journal of Nanomedicine, 2019, 14, 8627-8645.

[31] J. H. Jeon, J. H. Park, and T. Kim, Phenylboronic acid-conjugated cationic methylcellulose for hepatocellular carcinoma-targeted drug/gene co-delivery systems, Journal of Industrial and Engineering Chemistry, 2019, 75, 148-157.

[32] S. Tang, T. Wang, Q. Yong et al., Arabinogalactans from Larix principis-rupprechtii: An investigation into the structure-function contribution of side-chain structures, Carbohydrate Polymers, 2020, 227, 115354.

[33] B. Singh, S. Maharjan, C. Cho et al., Tuning the Buffering Capacity of Polyethylenimine with Glycerol Molecules for Efficient Gene Delivery: Staying In or Out of the Endosomes, Macromolecular Bioscience, 2015, 15(5), 622-635

[34] R. Shrestha, M. Elsabahy, K. L. Wooley, Endosomal escape and siRNA delivery with cationic shell crosslinked knedel-like nanoparticles with tunable buffering capacities, Biomaterials, 2012, 33(33), 8557-8568

[35] T. Kim, T. Rothmund, T. Kissel, and S. W. Kim, Bioreducible polymers with cell penetrating and endosome buffering functionality for gene delivery systems, Journal of Controlled Release, 2011, 152(1), 110-119.

[36] C. M. Jewell, and D. M. Lynn, Surface-mediated delivery of DNA: Cationic polymers take charge, Current Opinion in Colloid & Interface Science, 2008, 13(6), 395-402.

[37] J. Rejman, V. Oberle, I. S. Zuhorn, and D. Hoekstra, Size-dependent internalization of particles via the pathways of clathrin- and caveolae-mediated endocytosis, Biochemical Journal, 2004, 377(Pt 1), 159-169.

[38] J. J. Rennick, A. R. R. Johnston, and R. G. Parton, Key principles and methods for studying the endocytosis of biological and nanoparticle therapeutics, Nature Nanotechnology, 2021, 16, 266-276.

[39] M. S. Almeida, E. Susnik, B. Rothen-Rutishauser et al., Understanding nanoparticle endocytosis to improve targeting strategies in nanomedicine, Chemical Society Review Journal, 2021, 50, 5397-5434.

[40] E. Trofimenko, Y. Homma, M. Fukuda, and C. Widmann, The endocytic pathway taken by cationic substances requires Rab14 but not Rab5 and Rab7, Cell Reports, 2021, 37(5), 109945.

[41] D. Manzanares, and V. Cena, Endocytosis: The Nanoparticle and Submicron Nanocompounds Gateway into the Cell, Pharmaceutics, 2020, 12(4), 371.

[42] S. Gwak, C. Macks, S. Bae, N. Cecil, and J. S. Lee, Physicochemical stability and transfection efficiency of cationic amphiphilic copolymer/pDNA polyplexes for spinal cord injury repair, Scientific Reports, 2017, 7, 11247

[43] J. Park, K. Kim, S. Jeong, M. Lee, and T. Kim, Highly Osmotic Oxidized Sucrose-Crosslinked Polyethylenimine for Gene Delivery Systems, Pharmaceutics, 2021, 13(1), 87.

[44] J. Seo, S. Jeong, M. Lee, T. Kim, Zoledronic acid-loaded cationic methylcellulose polyplex nanoparticles for enhanced gene delivery efficiency and breast cancer cell killing effect, Applied Nanoscience, 2022, 12 (11), 3303-3314.

[45] O. S. Kolovskaya, T. N. Zamay, A. S. Kichkailo et al., Aptamer-Conjugated Superparamagnetic Ferroarabinogalactan Nanoparticles for Targeted Magnetodynamic Therapy of Cancer, Cancers, 2020, 12

(1), 216.

[46] N. Yoshinaga, S. Uchida, K. Kataoka et al., Induced packaging of mRNA into polyplex micelles by regulated hybridization with a small number of cholesteryl RNA oligonucleotides directed enhanced in vivo transfection, Biomaterials, 2019, 197, 225-267.

[47] I. Serrano-Sevilla, A. Artiga, J. M. Fuente et al., Natural Polysaccharides for siRNA Delivery: Nanocarriers Based on Chitosan, Hyaluronic Acid, and Their Derivatives, Molecules, 2019, 24(14), 2570.

[48] L. Galluzzi, I. Vitale, G. Kroemer et al., Molecular mechanisms of cell death: recommendations of the Nomenclature Committee on Cell Death 2018, Cell Death & Differentiation, 2018, 25, 486-541.

[49] T. V. Berghe, N. Vanlangenakker, P. Vandenabeele et al., Necroptosis, necrosis and sondary necrosis converge on similar cellular disintegration features, Cell Death & Differentiation, 2009, 17, 922-930.

초록

간세포성 암종 (HCC)은 사망률이 세 번째로 높은 암이다. HCC는 간암 세포에 과발현된 아시알로당단백질 수용체를 표적하여 치료제를 전달하는 방법을 통해 치료할 수 있다. 따라서 본 연구에서는, 아라비노갈락탄을 폴리에틸렌이민으로 개질하고 간암 표적화 유전자 전달체로서의 가능성을 평가하였다. 아라비노갈락탄의 사슬 구조에 적합한 'One pot method'를 새롭게 제시하여 폴리에틸렌이민 (분자량 10,000 Da)을 아라비노갈락탄에 접합하였다. ^{1}H NMR, FT-IR, 그리고 GPC 측정을 통해 성공적인 접합을 확인했다. 합성한 AGP 0.5X는 균일한 구형의 양이온성 폴리플렉스를 형성하였고, 세럼 단백질로부터 플리스미드 DNA를 보호하였다. AGP 0.5X를 고분자/유전자 무게비 10으로 설정하여 폴리플렉스를 형성하였을 때 HepG2에 대해 PEI25k 보다 높은 유전자 전달 효율을 나타냈고, 우수한 세포 내 거동을 나타냈다. 한편, 갈락토오스를 전처리 했을 때 유전자 전달 효율과 세포 침투 정도가 크게 낮아진 것을 통해 아시알로당당백질 수용체에 대한 AGP 0.5X의 표적 기능을 증명하였다. Bcl-2 siRNA와 폴리플렉스를 형성한 경우, Bcl-2 mRNA의 발현 정도가 크게 감소했고, 아폽토시스를 유도하여 간암 세포에 대한 항암 효과를 나타냈다. 이를 통해 AGP 0.5X의 간암 표적화 유전자 전달체로서의 새로운 가능성을 제시하였다.

주요어: 유전자 전달 시스템, 아라비노갈락탄, 폴리에틸렌이민, 간세포암, Bcl-2 siRNA

학번 : 2021-28034